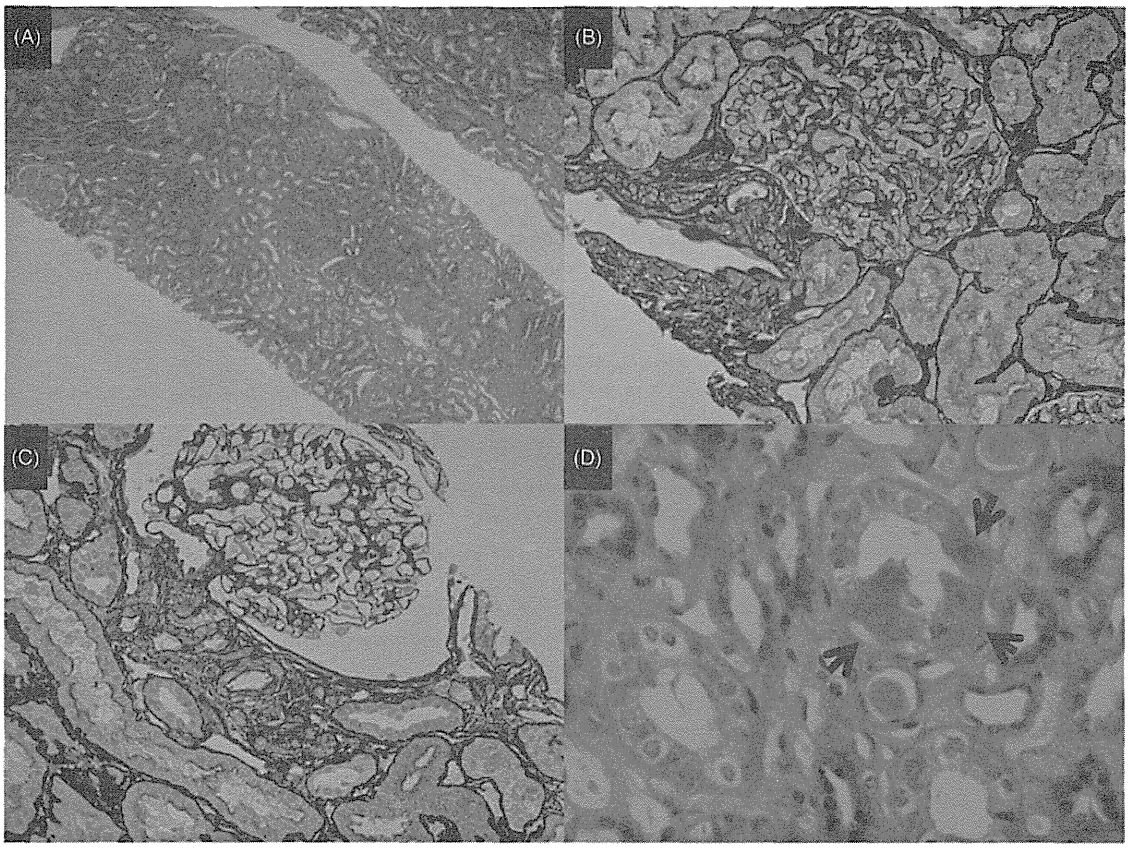


Figure 1. The light microscopic findings. (A) While globally sclerosed glomeruli and collapsed glomeruli were observed, the other glomeruli showed an almost normal appearance (Masson trichrome stain, original magnification ×40). (B) This glomerulus looks normal. However, the vascular smooth muscle cells are disorganized and enlarged (PAM-HE stain, original magnification ×200). (C) This glomerulus also looks normal, while the myocytes of the afferent arteriole are enlarged and their endothelium has slight hyalinosis (PAM-HE stain, original magnification ×200). (D) Granular swollen epithelial cells are indicated by arrows (Masson trichrome stain, original magnification ×400).

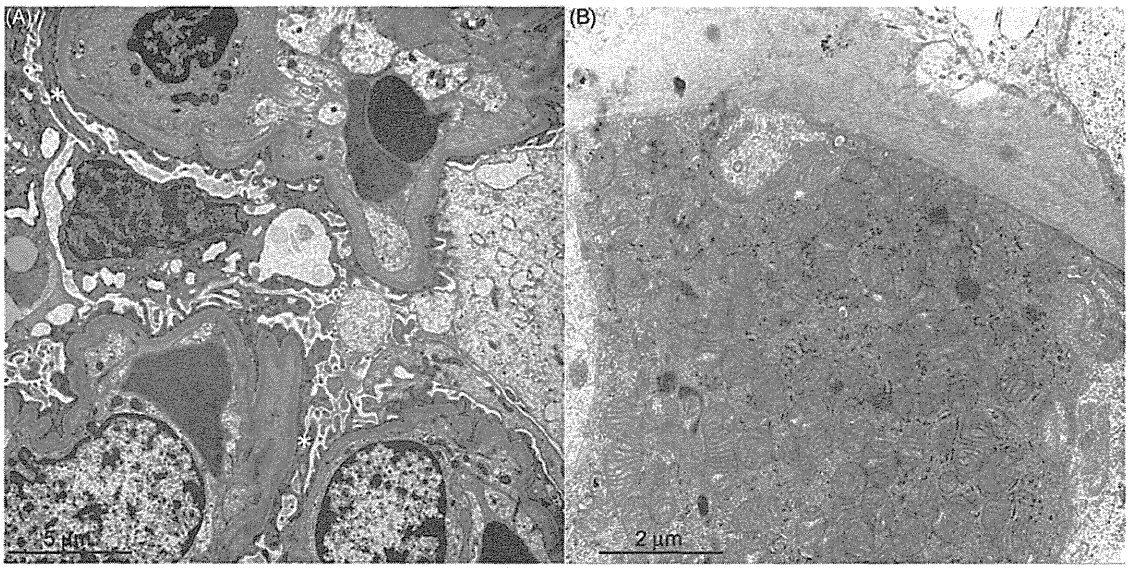


Figure 2. The electron microscopic findings. (A) The foot processes of podocytes are effaced (asterisks). (B) The granular swollen epithelial cells have increased numbers of mitochondria, a portion of which are enlarged, and some of which have cristae that have lost their normal structure.

blood cells by direct sequencing after obtaining both permission from our ethics committee and informed consent from the patient. As a result, a homoplasmic 7501 T>A replacement was detected (Figure 3). She had no symptoms of myopathy or encephalopathy, no history of stroke-like episodes or difficulty in hearing.

The echographic examination for her heart showed hypokinesis in the anteroseptum (Figure 4A, the ejection

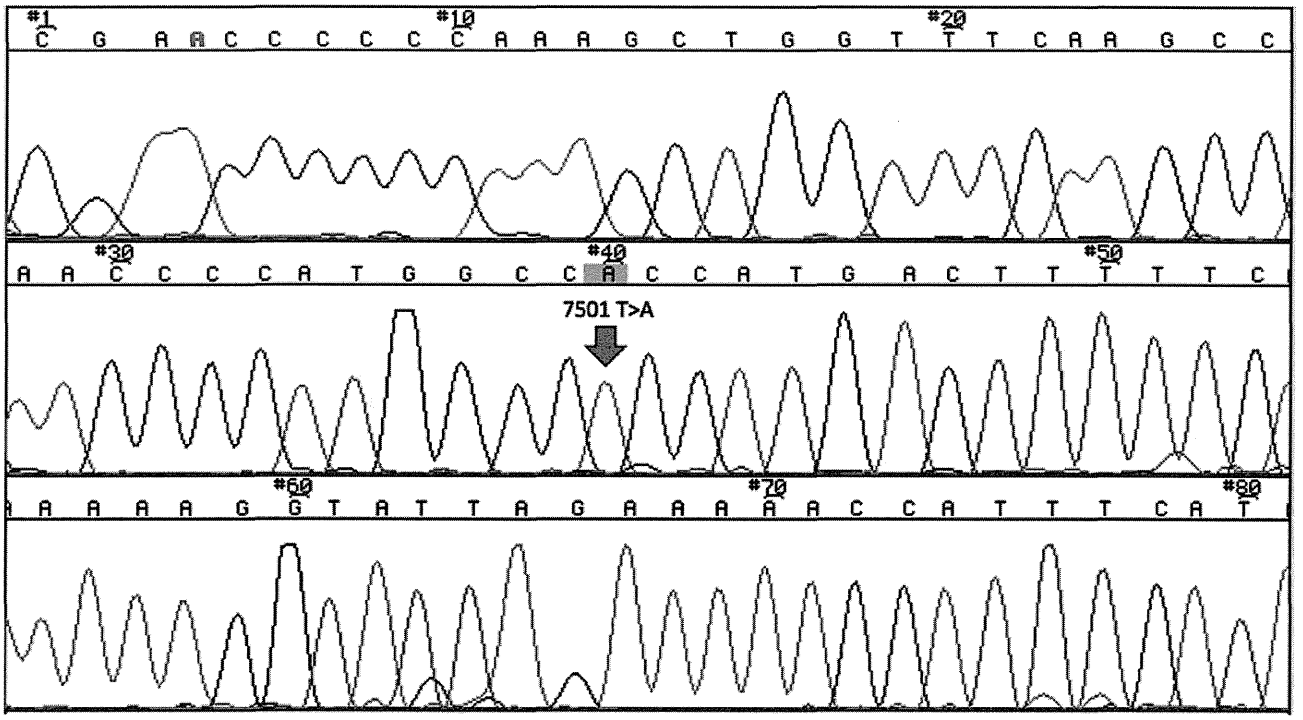


Figure 3. The results of the direct sequencing of mtDNA. A homoplasmic 7501 T > A variant in the tRNASer(UCN) was detected in the patient's blood sample.

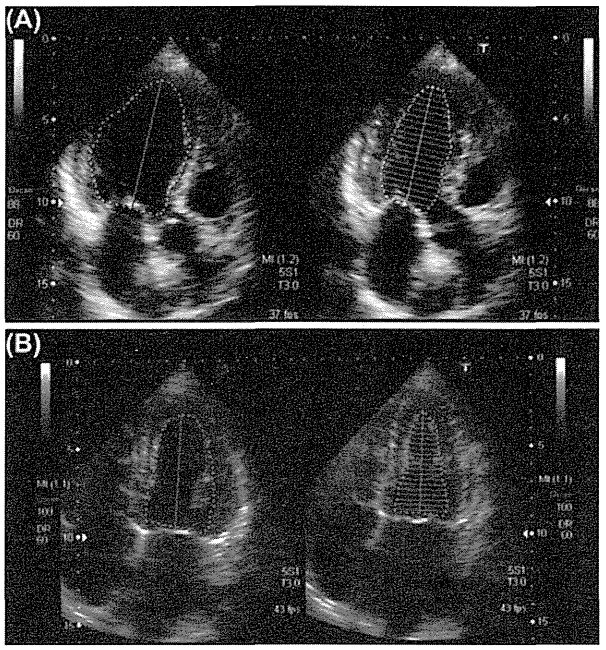


Figure 4. The B-mode echocardiogram. (A) The cardiac echogram on admission showed hypokinetic wall motion and anteroseptal hypokinesis. The ejection fraction determined by the modified Simpson's method was 45.9%. (B) One year after the prescription of a β-blocker, the cardiac echogram showed normal wall motion of the anteroseptum. The ejection fraction determined by a modified Simpson's method was 60.7%.

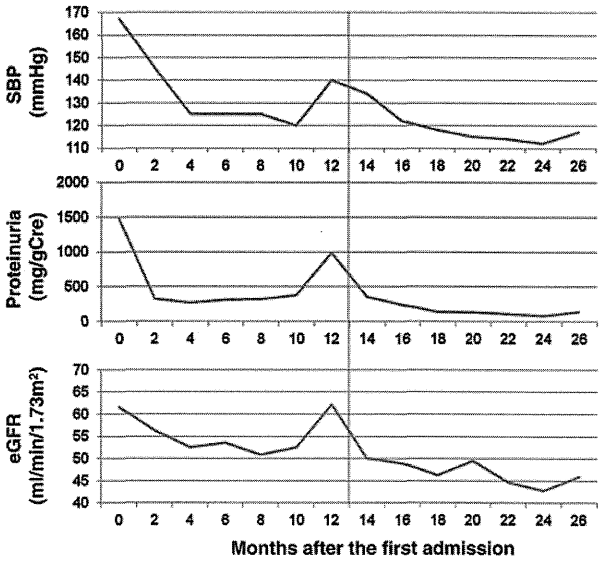


Figure 5. The changes of the systolic blood pressure (SBP), the degree of proteinuria and the estimated glomerular filtration rate (eGFR). The vertical line shows the time when the β-blocker was prescribed.

fraction by the modified Simpson's method was 45.9%). Therefore, she underwent coronary angiography. However, there were no abnormalities in her coronary arteries. Thereafter, we added a β-blocker, bisoprolol fumarate. After the prescription, the findings of cardiac echography changed to normal (ejection fraction by modified Simpson's method: 60.7%). Furthermore, the ST depression and inverted T waves on leads I, II, aVF, V4-6 recovered, although digitalis was given at same dose as at the first admission. Her proteinuria also decreased after the β-blocker, which was accompanied by a decrease in blood pressure (Figure 5). However, her estimated glomerular filtration rate has been gradually decreasing for the past two years. Although the

MPO-ANCA level was elevated at the first admission to our hospital, there has been no evidence of vasculitis (two years after the first admission).

## Discussion

Although we could neither find any FSGS lesions nor increased mitochondria in her podocytes, the renal pathology of this case showed similar changes to those of the nephropathy in patients with mitochondrial cytopathy in the following three points: progressive renal damage, abnormality of myocytes in the afferent arterioles and small arteries, and especially, the existence of GSECs in the tubules.[1–3] In addition, the concentrations of serum lactate and pyruvate were elevated. Therefore, we analyzed the patient for mtDNA mutations and consequently detected a homoplasmic 7501 T>A mtDNA variant.

It was reported that gene mutations of COQ2[6] and COQ6,[7] which are essential for COQ10 synthesis, cause FSGS. Coenzyme Q10 is an essential cofactor of the electron transport chain in the mitochondrial membrane. Therefore, mitochondrial function should be involved in glomerular podocyte function.[8] Furthermore, case reports of mtDNA mutations and deletions not only in FSGS but also in tubulointerstitial nephritis and tubulopathies have been gradually accumulating.[9] These reports indicate that mitochondria are likely involved in the pathogenesis of a considerable number of renal diseases, to a much greater extent than was considered previously.

In this study, a homoplasmic 7501 T>A variant in the tRNASer(UCN) was detected in our case of glomerulosclerosis with GSECs. This 7501 T>A replacement is currently classified as a normal variant in the MitoMap database (http://www.mitomap.org/MITOMAP). However, 7501 T>A should modify the secondary structure of the D-arm in the tRNASer(UCN) transcript.[10] The D-arm plays important roles in the stability of the transcript and the general rate of mitochondrial protein synthesis.[11] Furthermore, the 7501 T>A variant has been reported in patients with hearing loss. The 7501 T>C variant, which is also classified as a normal variant, was reported in a cardiomyopathy patient.[12] We again emphasize that it is not evident that the mitochondrial 7501 T>A variant truly has pathogenicity, and further tests, including functional studies, family studies and population studies are needed to verify its effects.

We propose another possible explanation for why the 7501 T>A variant causes glomerulosclerosis. As described above, the D-arm of the tRNASer(UCN) transcript is important for the general rate of mitochondrial protein synthesis. Thyroid hormone stimulates mitochondrial activity.[13] In this case, the patient also had Basedow's disease. Such a situation might make this mtDNA variant pathogenic, although it may not normally be pathogenic in healthy individuals. Interestingly, the patient's cardiac echogram showed hypokinesis in the anteroseptum wall. However, after the prescription of a β-blocker, the motion of the anteroseptum wall recovered. Therefore, although we cannot confirm the diagnosis of cardiomyopathy in this case, mitochondrial dysfunction as result of the 7501 T>A variant might be able to cause cardiomyopathy similar to the 7501 T>C variant.[12]

In this case, the first and the strongest reason why we suspected the involvement of mitochondria was the pathological finding of GSECs, even without any signs of mitochondrial cytopathy and without FSGS and an increase in the number of mitochondria in glomerular podocytes, which is characteristic of mtDNA mutations. Previously, GSECs have not been evaluated in routine clinical tests. This case suggests that GSECs can provide a clue to assess the etiopathogenesis of cryptogenic glomerulosclerosis and tubulopathy.

## Declaration of interest

The authors report no conflicts of interest. The authors alone are responsible for the content and writing of the paper.

This work was supported by the JSPS (Japan Society for the Promotion Science) KAKENHI Grant Number 80348276 to T. Imasawa, and a grant from the National Hospital Organization of Japan to T. I.

## References

1. Doleris LM, Hill GS, Chedin P, et al. Focal segmental glomerulosclerosis associated with mitochondrial cytopathy. *Kidney Int.* 2000;58:1851–1858.
2. Hotta O, Inoue CN, Miyabayashi S, et al. Clinical and pathologic features of focal segmental glomerulosclerosis with mitochondrial tRNALeu(UUR) gene mutation. *Kidney Int.* 2001;59:1236–1243.
3. Guéry B, Choukroun G, Noël LH, et al. The spectrum of systemic involvement in adults presenting with renal lesion and mitochondrial tRNA(Leu) gene mutation. *J Am Soc Nephrol.* 2003;14:2099–2108.
4. Kobayashi A, Goto Y, Nagata M, Yamaguchi Y. Granular swollen epithelial cells: A histologic and diagnostic marker for mitochondrial nephropathy. *Am J Surg Pathol.* 2010;34:262–270.
5. Ishii R, Imaizumi M, Ide A, et al. A long-term follow-up of serum myeloperoxidase antineutrophil cytoplasmic antibodies (MPO-ANCA) in patients with Graves disease treated with propylthiouracil. *Endocr J.* 2010;57:73–79.
6. Diomedi-Camassei F, Di Giandomenico S, Santorelli FM, et al. COQ2 nephropathy: A newly described inherited mitochondriopathy with primary renal involvement. *J Am Soc Nephrol.* 2007;18:2773–2780.
7. Heeringa SF, Chernin G, Chaki M, et al. COQ6 mutations in human patients produce nephrotic syndrome with sensorineural deafness. *J Clin Invest.* 2011;121:2013–2024.
8. Imasawa T, Rossignol R. Podocyte energy metabolism and glomerular diseases. *Int J Biochem Cell Biol.* 2013;45:2109–2118.
9. O'Toole JF. Renal manifestations of genetic mitochondrial disease. *Int J Nephrol Renovasc Dis.* 2014;7:57–67.
10. Mutai H, Kouike H, Teruya E, et al. Systematic analysis of mitochondrial genes associated with hearing loss in the Japanese population: dHPLC reveals a new candidate mutation. *BMC Med Genet.* 2011;12:135.
11. Möllers M, Maniura-Weber K, Kiseljakovic E, et al. A new mechanism for mtDNA pathogenesis: impairment of post-transcriptional maturation leads to severe depletion of mitochondrial tRNASer(UCN) caused by T7512C and G7497A point mutations. *Nucleic Acids Res.* 2005;33:5647–5658.
12. Zaragoza MV, Fass J, Diegoli M, Lin D, Arbustini E. Mitochondrial DNA variant discovery and evaluation in human cardiomyopathies through next-generation sequencing. *PLoS One.* 2010;5:e12295.
13. Wrutniak-Cabello C, Casas F, Cabello G. Thyroid hormone action in mitochondria. *J Mol Endocrinol.* 2001;26:67–77.

OPEN ACCESS Freely available online

PLOS ONE

# Evolution of Mitochondrial Power in Vertebrate Metazoans

**Yasuhiro Kitazoe[1]*, Masashi Tanaka[2]**

**1** Center of Medical Information Science, Kochi Medical School, Nankoku, Kochi, Japan, **2** Department of Genomics for Longevity and Health, Tokyo Metropolitan Institute of Gerontology, Tokyo, Japan

## Abstract

***Background:*** Basal metabolic rate (*BMR*) has a very strong body-mass (*M*) dependence in an individual animal group, and *BMR* per unit mass (*msBMR*) converges on a markedly narrow range even across major taxonomic groups. However, it is here a basic question in metazoan biology how much *BMR* per unit mitochondrion (*mtBMR*) changes, and then whether *mtBMR* can be related to the original molecular mechanism of action of mt-encoded membrane proteins (MMPs) playing a central role in cellular energy production.

***Methodology/Principal Findings:*** Analyzing variations of amino-acid compositions of MMPs across 13 metazoan animal groups, incorporating 2022 sequences, we found a strong inverse correlation between Ser/Thr composition (*STC*) and hydrophobicity (*HYD*). A majority of animal groups showed an evolutionary pathway of a gradual increase in *HYD* and decrease in *STC*, whereas only the deuterostome lineage revealed a rapid decrease in *HYD* and increase in *STC*. The strongest correlations appeared in 5 large subunits (ND4, ND5, ND2, CO1, and CO3) undergoing dynamic conformational changes for the proton-pumping function. The pathway of the majority groups is well understood as reflecting natural selection to reduce *mtBMR*, since simply raising *HYD* in MMPs (surrounded by the lipid bilayer) weakens their mobility and strengthens their stability. On the other hand, the marked decrease in *HYD* of the deuterostome elevates *mtBMR*, but is accompanied with their instability heightening a turnover rate of mitochondria and then cells. Interestingly, cooperative networks of interhelical hydrogen-bonds between motifs involving Ser and Thr residues can enhance MMP stability.

***Conclusion/Significance:*** This stability enhancement lowers turnover rates of mitochondria/cells and may prolong even longevity, and was indeed founded by strong positive correlations of *STC* with both *mtBMR* and longevity. The lowest *HYD* and highest *STC* in Aves and Mammals are congruent with their very high *mtBMR* and long longevity.

**Citation:** Kitazoe Y, Tanaka M (2014) Evolution of Mitochondrial Power in Vertebrate Metazoans. PLoS ONE 9(6): e98188. doi:10.1371/journal.pone.0098188

**Editor:** Yidong Bai, University of Texas Health Science Center at San Antonio, United States of America

**Received** March 11, 2014; **Accepted** April 25, 2014; **Published** June 9, 2014



**Data Availability:** The authors confirm that all data underlying the findings are fully available without restriction. All data are in the manuscript and accession numbers of amino acid sequences are in the supplemental file S1.

**Funding:** This work was supported by Grants-in-Aid for Scientific Research from the Ministry of Education, Culture, Sports, Science, and Technology of Japan (A-22240072 B-21390459 and C-21590411 to M.T.) by Grants-in-Aid for Research on Intractable Diseases (Mitochondrial Disorders) from the Ministry of Health, Labor, and Welfare of Japan (23-016, 23-116 and 24-005 to M.T.) and by grants for scientific research from the Takeda Science Foundation (to M.T.). The funders had no role in study design, data collection and analysis, decision to publish, or preparation of the manuscript.

**Competing Interests:** The authors have declared that no competing interests exist.

* E-mail: kitazoeyasuhiro@yahoo.co.jp

## Introduction

Because the basal metabolic rate (*BMR*) is a fundamental currency to sustain metazoan life, it must be profoundly relevant to the mt power in energy production. However, its strong mass (*M*)-dependence makes unclear the existence of a relationship between *BMR* and this mitochondrial (mt) energy power across major taxonomic groups. A recent allometric study reports that the mass specific BMT (*msBMR*) converges on a markedly narrow range in these groups [1]. This viewpoint of the normalized energy inclines us to convert *msBMR* into the mt *BMR* (*mtBMR*) per unit mitochondrion which stands for the mt energy power, since the conversion can be done when *msBMR* includes the falling effect of the mt density (the mean number of mitochondria per unit cell) with increasing *M* [2], [3]. It is intriguing to estimate how much *mtBMR* changes across taxonomic groups, because recent structural studies report a high degree of sequence conservation of the membrane integral central subunits [4], [5], the mechanism of which is therefore likely to be similar throughout species [6].

The first step to relate *mtBMR* to the mt energy production power is to investigate the molecular structure of mt-encoded membrane proteins (MMPs) by using a number of amino acid sequences which are available in the NCBI database [7] (the accession numbers of these sequences are listed up in Table S1). The great majority of MMPs belongs to the 3 proton-pumping complexes of I, III and IV. Recent structural studies suggest that proton translocation in complex I requires large dynamic conformational changes across several subunits [6], [8], [9]. Likewise, the two large subunits of complex IV, i.e., CO1 and CO3, transfer protons across the membrane via conformational changes induced by electron transport [10–12].

MMPs are mostly embedded in the hydrophobic environment of the lipid bilayer, and their amino acid composition is primarily hydrophobic, with approximately 90–95% of these amino acids

being non-polar. Therefore, the degree (mobility) of their conformational changes much depends on hydrophobicity (*HYD*): Raising *HYD* weakens their mobility and strengthens their stability according to the trade-off relation between mobility and stability [13]. Interestingly, a recent study of membrane proteins reports that the dynamic conformational stability of membrane helices can be typically enhanced by cooperative networks of interhelical hydrogen bonds between moderately polar residues, notably Ser and Thr [13–15]. The above-mentioned two features of *HYD* and Ser/Thr composition (*STC*) allow us to conceive a basic scenario of the metazoan evolution that lowering *mtBMR* (on the basis of the multicellular effect) requires less dynamic conformational changes of MMPs which induce an increase in *HYD* and a decrease in *STC*.

Here we report that most members of major animal groups follow this evolutionary scenario. However, the deuterostome lineage reveals the converse, i.e., rapid increases in *STC* and *mtBMR*, and a rapid decrease in *HYD* toward the endpoints (Aves and Mammals) of this lineage. Aves and Mammals seem ready to power up the mt energy by activating dynamical conformational changes of MMPs and still then enhance stability (durability) of them by increasing helix-helix interactions. This durability lowers turnover rates of mitochondria and cells, and may prolong longevity of organisms. Indeed, a strong correlation between *STC* and maximum lifespan (*MLS*) (observed in a previous vertebrate analysis [16]) was found to extend as a global rule beyond vertebrates across metazoans.

## Materials and Methods

### Derivation of *mtBMR* from *msBMR*

The allometric scaling law provides a very strong correlation between *BMR* and *M* in each animal group, and is expressed as $BMR = C \cdot M^{\alpha}$ with an allometric exponent $\alpha$ and constant *C*. Makarieva et al. [1] well described a variation of *BMR* data across different animal groups by using *BMR* per unit mass (*msBMR*), i.e., $msBMR = C \cdot M^{-(1-\alpha)}$

They reported that *msBMR* data across dramatically different life forms converge on a markedly narrow range. This unit-mass representation of *msBMR* implicitly means that an organism is approximately regarded as a homogeneous matter of standard (representative) cells: the number of cells in unit mass and also that of mitochondria (the mt density) in unit cell are invariant, respectively, although, in practice, metabolically active cells, such as those of the liver, kidneys, muscles, and brain, have hundreds or thousands of mitochondria [17]. Therefore, *msBMR* is proportional to *BMR* per unit cell (we put this proportional constant equal to 1.0). Next, to get *BMR* per unit mitochondrion, we divide *msBMR* by the factor $M^{-\beta}$ which takes into account the decreasing effect of the mt density with increasing *M* [2], [3]. Then we have $mtBMR = (C/D) \cdot M^{-(1-\alpha-\beta)}$, which means that *mtBMR* decreases with increasing *M* more slowly than does *msBMR*. In this paper, we express *mtBMR* as follows: $mtBMR = C \cdot M^{-(1-\alpha)/F}$. Here, *F* is with a new parameter to adjust the allometric scaling effect of the *M*-dependence. For simplicity, we put the proportional constant *D* equal to 1.0, since the value of $F = 1.0$ corresponds to *msBMR*. In a previous mammalian analysis, the value of $F = 3.0$ was selected as providing the strongest correlation between *mtBMR* and *MLS* [16]. In the present analysis, we redefine *M* as the mean value of the individual body masses in each animal group, to examine a relationship between *mtBMR* and amino acid compositions of MMPs in major taxonomic groups.

### Data retrieval

To select a hydrophobic domain in MMPs, we applied the primary structure analysis (ExPASy Proteomics Server; http://www.expasy.ch/), using a standard model for the hydrophobic score (*HYDSC*) given by Cowan and Whittaker [18]. We calculated the moving average, *S*(n), of *HYDSC*(m; m takes n-1, n, and n+1) around the n-th amino acid site in a protein and obtained a smooth function *S*(n) of n by repeating this procedure. As a result, *HYD* was defined as the average value of *S*(n) with *S*(n) >0.0 in all or selected proteins of a given species. The obtained *HYD* is suitable for examining correlations with other quantities of present interest, such as amino acid compositions and lifespan. We predicted the helix domain of MMPs by using SOSUI and TMHMM servers [19], [20].

## Results

### A) *HYD-TC* correlation within respective MMPs

By including 13 metazoan animal groups with many amino acid sequences (more than 20) in the NCBI database [7], we analyzed 13 MMPs with a score $S>0$ for their hydrophobic domain (Materials and Methods). As a result, we selected 4 MMP variables (*HYD, STC, TC* and *CC*) of amino acid compositions as having significant correlations with one another, and found that *HYD-TC* provided an especially strong correlation. Here, TC and CC denote the Thr and Cys compositions, respectively. Table 1 shows a list of MMPs in the order of strong correlations. The 3 large subunits of ND4, ND5, and ND2 in complex I appeared as the first group with the largest $R^2$-values ($R^2>0.86$). Likewise, 2 large subunits of CO1 and CO3 in complex IV appeared as the second group (with $R^2>0.78$). These subunits just correspond to the proteins which require dynamic conformational changes for proton translocation [6], [8], [9]. The *TC-CC* correlation was appreciable in only these 2 proton-pumping complexes (with $R^2>0.40$) undergoing dynamic conformational changes in their helices.

### B) Correlations between the MMP variables (*HYD, STC, TC* and *CC*)

We investigated the intra-correlations between the MMP variables, by using the following 5 sets of proteins according to the order of strong correlations shown in Table 1: **1**) 3-protein set (ND4, ND5, ND2), **2**) 4-protein set (ND4, ND5, ND2, ND1), **3**) 5-protein set (ND4, ND5, ND2, CO1, CO3), **4**) 6-protein set (ND4, ND5, ND2, CO1, CO3, ND1), and **5**) 7-protein set (ND4, ND5, ND2, CO1, CO3, ND1, CYTB). Here, the 3-protein set included 39% of the total site number of the complete amino acid sequence in humans, and the 7-protein set, 76% of it. The 7-protein set did not include ND3 and ATP8 with small numbers of helices (3 or less in humans). As seen in Table 2, *TC* provided predominantly strong correlations with *HYD* in all protein sets, and the strongest correlation ($R^2 = 0.9$) in the 5-protein set (Figure 1). In addition to this, *TC-CC, HYD-CC* and *HYD-STC* showed appreciable correlations. Here, we used the average values of *TC* and *HYD* in each animal group, in order to describe the correlation pattern lucidly (the raw data without the averaging procedure also showed a strong correlation of $R^2 = 0.9$ (Figure S1). As a result, the *TC*-values in Aves and Eutheria with very high *BMR* were 2.5 fold larger than those of Nematoda and Platyhelminthes with very low *BMR*, and the *HYD* values of the former were decreased by about 22% compared with those of the latter. The validity of these estimations of *TC* and *HYD* was supported by speculating the *TC* and *HYD* distributions in the helix domain of the above-mentioned 4 animal groups (Figure 2).

**Table 1.** *HYD-TC* and *TC-CC* correlations ($R^2$) within respective proteins.

| | ND4 | ND5 | ND2 | CO1 | CO3 | ND1 | ND3* | ATP8* | CYTB | ND4L* | CO2* | ATP6* | ND6* |
|---|---|---|---|---|---|---|---|---|---|---|---|---|---|
| HYD-TC | 0.89 | 0.89 | 0.87 | 0.81 | 0.78 | 0.68 | 0.68 | 0.65 | 0.60 | 0.58 | 0.57 | 0.37 | 0.03 |
| TC-CC | 0.60 | 0.61 | 0.64 | 0.41 | 0.49 | 0.38 | 0.32 | 0.25 | 0.26 | 0.11 | 0.29 | 0.63 | 0.42 |

The * symbol denotes 2 subunits with weak correlations (ATP6 and ND6) and 4 subunits with small numbers (3 or less in humans) of helices (ND3, ATP8, ND4L, and CO2). The analysis includes the following 13 metazoan animal groups: Porifera, Cnidaria, Mollusca, Crustacea, Hexapoda, Chelicerata, Nematoda, Platyhelminthes, Echinodermata, Fishes, Amphibia, Eutheria, and Aves.

doi:10.1371/journal.pone.0098188.t001

## C) Correlations between MMP variables and total site number of amino acids

We found that the total site number (*TSN*) of amino acids in a protein set steadily changes across the 13 animal groups (by 20% as a whole) and is a good index to describe the mutually contrasting evolutionary pathways of *TC* and *HYD* in metazoans (Figure 3). The *TSN* order of the animal groups (their relative *TSN*-dependence) was invariant in all protein sets (Figure S2). As a result, *TSN* strongly correlated with *TC* and *HYD*, when the deuterostomes were excluded (Table 2). Indeed, *TC* gradually decreased with decrease in *TSN* of many animal groups except for the deuterostomes (Figure 3, blue regression line), whereas *HYD* increased with a decrease in *TSN* (Figure 3, red regression line). On the other hand, *TC* and *HYD* in the deuterostome lineage presented rapidly increasing and decreasing trends with a decrease in *TSN* towards the terminal branch of Aves, clearly splitting from the 2 regression lines. This splitting pattern could be identified by looking at the *TC-HYD* relationship of Figure 1, because the non-linear regression curve **A** ($TC = 0.429 \cdot HYD^{-4.241}$ with $R^2 = 0.90$ as a whole) was decomposed into a steep slope dotted-line **B** ($TC = -65.66 \cdot HYD + 41.75$ with $R^2 = 0.92$) for the deuterostomes and a slow slope dotted-line **C** ($TC = -18.32 \cdot HYD + 14.92$ with $R^2 = 0.89$) for the other animal groups. The splitting pattern of Figure 3 became compatible with a molecular (rRNA)-based phylogeny [21], in the point that the tree starts with the root of Porifera and splits into the two lineages of Deuterostomia and Protostomia via Cnidaria. In this way, the *TC-HYD* relationship globally reflected the evolutionary pathway of metazoans.

## D) Correlations between MMP variables and *mtBMR*

We examined correlations between *mtBMR* and MMP variables (*TC*, *STC*, and *HYD*) at the same mt function level, by increasing the *F* value from 1.0 (corresponding to *msBMR*) to infinity. The *mtBMR* values were estimated by extending *msBMR* in the respective animal groups (Materials and Methods). Since the data on metazoans with low *BMR* were very limited, we here applied the recent data reported by Makarieva et al. [1] and also the AnAge database for vertebrates (Table S2). We investigated the correlation between *STC* and *mtBMR* by changing the *F*-value included in this quantity 1 from 1.0 to infinity (Materials and Methods). Then we found that excluding the *M*-dependence of *mtBMR* with $F = \infty$ provides the strongest correlation (Figure S3). As a result, *mtBMR* correlated significantly with all MMP variables (*STC*, *TC*, *HYD*, and *CC*) in almost all of the protein sets, whereas *msBMR* weakly correlated with *STC* in only the 5-, 6-, and 7-protein sets. Here, *mtBMR* showed an especially strong correlation with *STC* in all protein sets (Table 2), since *STC* well describes vertebrates [16] and this analysis includes relatively many vertebrates. Figure 4A demonstrates a typical case of the 3-protein set, which shows a significant *STC-mtBMR* correlation with markedly high *mtBMR*–values in Aves and Eutheria. We here note that the *STC-msBMR* correlation was not strong with $R^2 = 0.28$.

## E) Correlations of *STC* with *MLS*

The significant correlation between *STC* and *mtBMR* prompted us to examine the relationship between *STC* and *mtBMR·MLS*, because *mtBMR·MLS* corresponds to the total consumption energy per mitochondrion during the time (*MLS*) and may therefore be interpreted as a performance of the mt function. Here, *MLS* is redefined as the mean value of the individual MLSs in an animal group. By taking account of this time effect, the *STC-mtBMR·MLS* correlation ($R^2 = 0.81$) became much stronger than the *STC-*

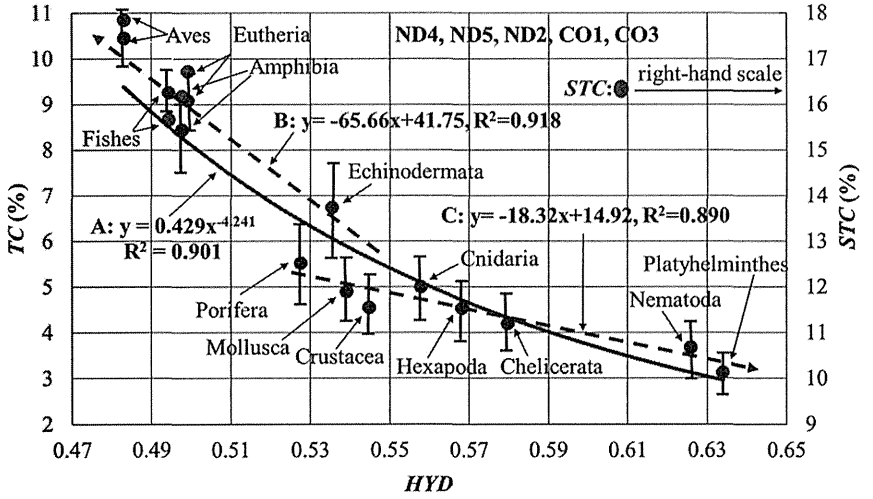


**Figure 1. Global relationship between *TC* and *HYD* in MMPs of metazoan animals.** Solid circles represent the average values of *HYD* and *TC* in each animal group, with the hydrophobic score S>0 (see Materials and Methods). The red circles show the *STC* values, which well describe the vertebrate lineage [16]. Such a strong correlation was also obtained by analyzing all 13 proteins (Figure S1). The correlation is totally well reproduced by a non-linear function (**A**: $TC = 0.429 \cdot HYD^{-4.2045}$ with $R^2 = 0.901$), but it can be separately expressed by 2 regression lines with different slopes (**B**: the dotted line for the deuterostomes with $R^2 = 0.918$) and (**C**: the dotted line for the other groups with $R^2 = 0.890$). The error range of the x-axis (*HYD*) in an animal group can be estimated by moving the regression curve **A** in parallel along the y-axis so that the y-value of this curve may be equal to that of the solid circle of the group, since this error range of *HYD* may be roughly given by the x-axis values of the curve corresponding to the error range of the y-axis (*STC*).
doi:10.1371/journal.pone.0098188.g001

*mtBMR* correlation ($R^2 = 0.64$) (the 3-protein set in Table 2), and separated vertebrates from other animal groups (Figure 4B). Figure 4C demonstrates a strong *STC-MLS* positive correlation ($R^2 = 0.71$) in the 3-protein set, and we found significant correlations between the MMP variables and *MLS* (Table 2). The *CC-MLS* correlation is likely to be related to oxidative damage to mitochondrial proteins or mtDNA [22–24], but was always weaker than the *STC-MLS* correlation in all protein sets (Table 2).

## Discussion

### Gradual increase in *HYD* for natural selection in many animal groups

A recent structural elucidation of ion channels in transmembrane proteins has provided evidence that these proteins undergo conformational changes during their function [13]. An easily understandable strategy of ecological and natural selection in metazoans is a reduction in their *BMR* by utilizing the multicellular effects of allometric scaling. Indeed, in many animal groups except for the deuterostomes, *HYD* and *TC* gradually

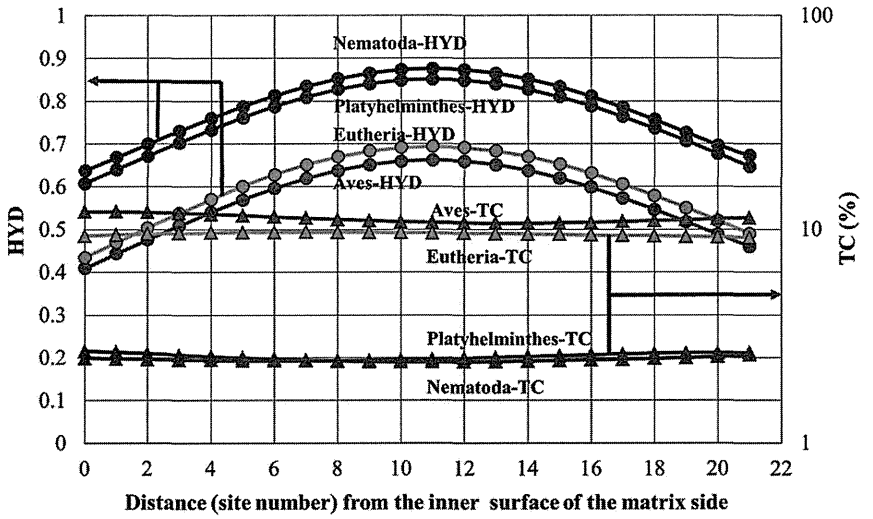


**Figure 2. *HYD* and *TC* distributions in the mt inner membrane of ND2, ND4 and ND5.** Four animal groups were selected as providing extreme situations of the hydrophobic distribution. This result was obtained by using SOSUI WWW server [19] and TMHMM Server [20] for the prediction of the secondary structure of proteins.
doi:10.1371/journal.pone.0098188.g002

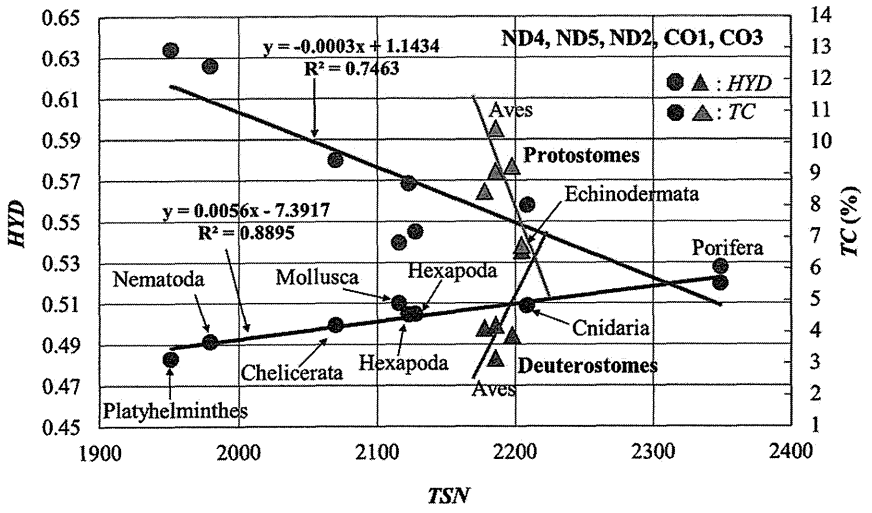


**Figure 3. *HYD* and *TC* versus *TSN*.** The regression lines for Deuterostomes and those for Protostomes were estimated separately. *HYD* and *TC* are expressed on the left and right ordinates, respectively.
doi:10.1371/journal.pone.0098188.g003

increased and decreased, respectively, with decrease in *TSN* (Figure 3). Here, the decrease in *TC* correlated with that in *mtBMR* (Figure 4A), since less dynamic mobility and weaker stability in MMPs balance each other for the mt function. The expression of animal groups in terms of *HYD* and *TC/STC* may be consistent with their phylogenetic tree. Indeed, the order of animal groups along the *TSN-HYD* regression line in Figure 3 became globally compatible with the branching pattern projected on the evolutional pathway from Porifera toward Platyhelminthes in the molecular (rRNA)-based phylogeny reported by Adoutte et al. [21]. This compatibility was supported by the neighbor-joining tree [25] in terms of *TSN* and *TC* (Figure S4) and also by a multidimensional vector space method of tree building (Figure S5) [26], [27]. However, the 2 lowest values of *TSN* were occupied by Platyhelminthes (Acoelomata) and Nematoda (Pseudocoelomata). The life style of these two groups seems to be closely related to each other, since they live mostly in anaerobic environments. On the other hand, the molecular-based phylogeny coupled Platyhelminthes with Mollusca (Coelomata) as Lophotropods. Apart from this problem, the gradual increase in *HYD* of MMPs well explains the evolutionary pathway of ecological selection to strengthen their stability in many animal groups except for the deuterostomes.

## Increase in *STC* and decrease in *HYD* for adaptive evolution in Deuterostomes

The marked decrease in *HYD* and increase in *STC* of the deuterostome lineage are quite interesting (Figure 3), because they are likely to break the ordinary trade-off relationship rule between mobility and stability as being well understood in the evolutionary pathway of many other animal groups. These mutually reverse pathways of *HYD* and *STC* in the 2 large animal groups are far from regarding mtDNA as the neutral marker long held to be [28], cannot be explained by the nucleotide mutation pressure [29–32], and are therefore a strong evidence of adaptive evolution at the mt genome level. Another reverse process was previously observed in vertebrate marine animals such as cetaceans and alligators which returned from the land to water, because these animal groups underwent the evolutionary pathway of an increase in *HYD* and a decrease in *STC* toward Fishes in contrast to that of the decrease in *HYD* and increase in *STC* [16].

## Marked decrease in *HYD* and increase in *STC* heighten mt function in vertebrates

To pursue the biological meaning of the decrease in *HYD* and increase in *STC* in the deuterostome lineage, we introduced the quantity, *mtBMR*, being an energetic function at the same mt level as *HYD* and *STC*. Indeed, *mtBMR* was correlated negatively with *HYD* and positively with *STC* (Table 2). Figure 4A demonstrates a typical *STC-mtBMR* correlation ($R^2 = 0.64$) in the 3-protein set (a linear combination of *STC* and *HYD* provided a stronger correlation ($R^2 = 0.77$) with *mtBMR*). The marked decrease in *HYD* supports the appearance of a very large *mtBMR* in Aves and Eutheria, since a highly active mt-function can be attained by realizing MMPs with greater conformational freedom. However, on the other hand, higher MMP instability induced by this greater freedom heightens turnover rates of mitochondria, which requires a higher cost to reproduce a large number of them within cells. Furthermore, spatial constraints in metazoan tissues make it difficult for organisms to develop much higher power by simply accumulating more mitochondria, because mitochondria in metabolically active cells (such as those of the liver and brain) of, for example, humans make up 40 percent of the cytoplasm [17]. In this situation, the marked increase in *STC* in MMPs of Aves and Eutheria must be a critical condition to compensate or overcome their instability.

## The reason why Ser and Thr residues can enhance dynamic stability of MMPs

Interestingly, membrane proteins have an outstanding feature of being able to strengthen their dynamic stability by interhelical interactions between motifs involving moderately polar residues such as Ser and Thr [13–15]. Indeed, the decrease in *HYD* and increase in *STC* in Aves and Eutheria were markedly large within the membrane itself, as is well understood by comparing their differences between Aves/Eutherians and Platyhelminthes/Nematoda (Figure 2). It is therefore likely that the increase in *STC* corresponds to increased hydrogen bonding between helices, within and between subunits, as pointed out by Dawson et al. [15] and Hildebrand et al. [13]. Because Ser and Thr residues are small and only moderately polar, helical structures tend to be stabilized by cooperative networks of interhelical hydrogen bonds. In a

**Table 2.** Correlations ($R^2$) between the pairs of variables (*HYD*, *TC*, *STC*, *CC*, *TSN*, *mtBMR*, *msBMR* and *MLS*).

| | | 3 proteins | 4 proteins | 5 proteins | 6 proteins | 7 proteins | mean |
|---|---|---|---|---|---|---|---|
| | | <39%> | <47%> | <59%> | <66%> | <76%> | |
| *TC-HYD* | N | 0.8898 | 0.8939 | 0.8997 | 0.8958 | 0.8867 | 0.89318 |
| *TC-CC* | N | 0.6554 | 0.6916 | 0.6994 | 0.7264 | 0.6691 | 0.68838 |
| *HYD-CC* | P | 0.5295 | 0.6081 | 0.6367 | 0.5449 | 0.5337 | 0.57058 |
| *HYD-STC* | N | 0.5052 | 0.4803 | 0.2992 | 0.3503 | 0.3151 | 0.3901 |
| *STC-CC* | N | 0.2387 | 0.2298 | 0.209 | 0.1887 | 0.1551 | 0.20426 |
| *TSN-TC* | P | 0.9232 | 0.9014 | 0.8907 | 0.8019 | 0.6699 | 0.83742 |
| *TSN-HYD* | N | 0.7591 | 0.7364 | 0.7484 | 0.6491 | 0.7171 | 0.7221 |
| *STC-*ln*(mtBMR)* | P | 0.6434 | 0.6483 | 0.7048 | 0.6762 | 0.6751 | 0.66956 |
| *TC-*ln*(mtBMR)* | P | 0.4999 | 0.4995 | 0.4948 | 0.5159 | 0.5316 | 0.5083 |
| *HYD-*ln*(mtBMR)* | N | 0.3403 | 0.3206 | 0.3547 | 0.3379 | 0.3574 | 0.34218 |
| *CC-*ln*(mtBMR)* | N | 0.4041 | 0.3441 | 0.3401 | 0.3184 | 0.2851 | 0.33836 |
| *STC-*ln*(msBMR)* | P | 0.1937 | 0.1979 | 0.2804 | 0.2514 | 0.2428 | 0.23324 |
| *STC-*ln*(MLS)* | P | 0.7065 | 0.6861 | 0.5691 | 0.5691 | 0.5687 | 0.6944 |
| *CC-*ln*(MLS)* | N | 0.3732 | 0.3962 | 0.3447 | 0.3667 | 0.3441 | 0.3654 |
| *STC-*ln*(mtBMR·MLS)* | P | 0.8133 | 0.8052 | 0.7737 | 0.7561 | 0.7551 | 0.78068 |

<n> denotes that *TSN* of each protein set occupies the n % of that of the complete amino acid sequence in Human. P and N stand for the positive and negative correlations, respectively. The best results in the respective correlation croups are denoted by italics.

doi:10.1371/journal.pone.0098188.t002

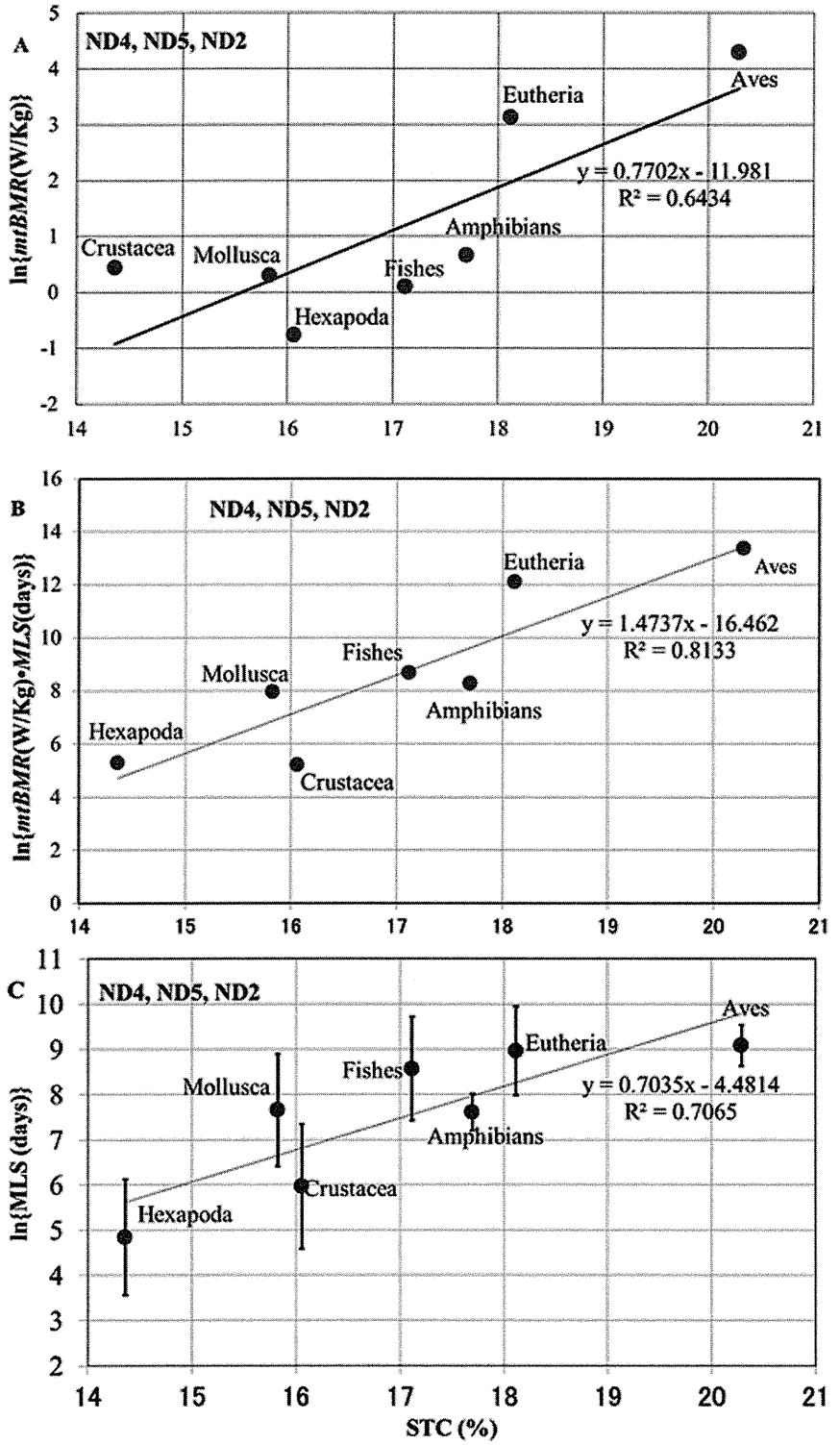


**Figure 4. Relationships of *STC* with *mtBMR* (A), *mtBMR*·*MLS* (B), and *MLS* (C).**
doi:10.1371/journal.pone.0098188.g004

previous paper [16], we showed that the short-range force of hydrogen bonds (1–2 Å) can be extended 2 to 3-fold (on average) by dynamic conformational changes in MMPs, because the relative distance of hydrogen bonding oscillates with the average amplitude R around R. Such a long-range potential amplifies the probability of interhelical interactions (in three-dimensional space) between cooperative networks of hydrogen bonds between motifs involving Thr or Ser residues. We envisage that such dynamic interactions could enable rapid resonance between metastable conformational states in MMPs, which have individual enzyme turnover rates of tens to hundreds of electrons per second [33]. In contrast, other types of hydrogen bonding, such as Cα-H---O

hydrogen bonding between Gly and Ala residues and the helical backbone, produce more rigid structures [13].

## Proton-pumping machinery and dynamic conformational changes in MMPs

Three large subunits (ND2, ND4 and ND5) in complex I provided the strongest correlations between *TC* and *HYD* (Table 1), which were further correlated with *mtBMR* (Table 2). These subunits exhibit homology with sodium-proton antiporters and are known to be part of the proton pumping machinery of complex I [34]. Structural models of complex I suggest that electron transfers in the hydrophilic matrix arm are coupled to proton translocation in the membrane arm: a redox-dependent conformational change around the Q-site is transmitted to the 3 antiporter-like proton-pumping subunits (ND2, ND4 and ND5). In this way, proton translocation in complex I requires dynamic conformational changes across several subunits [4], [5], [8], [9]. Likewise, the 2 large subunits (CO1 and CO3) of complex IV, which form the second group of the strong *TC-HYD* correlations, may transfer protons across the membrane via conformational changes induced by electron transport [10], [11]. A similar relationship is also true for the proton-pumping subunits in complex III (CYTB), which is directly involved in proton-pumping via the Q-cycle. The precise mechanism of proton pumping via the Q cycle is uncertain while shuttling electrons and protons across the membrane implies a lower requirement for dynamic conformational changes in CYTB. We do indeed report a less tight correlation between *HYD* and *TC* in CYTB (Table 1). From the above-mentioned arguments, we speculate that the marked decrease in *HYD* and increase in *STC* (*TC*) in Aves and Eutheria arranged a fundamental condition to afford the powerful and robust proton-pumping machinery of complexes I and IV in these groups.

## The reason why *STC* is relevant to *mtBMR* and *MLS*

The mt energy power profoundly influenced the origin and evolution of the eukaryotic cell [35], [36], and also must be closely associated with *BMR* to sustain organismal life. We noticed that variations of *mtBMR* across the different animal groups may be shielded by the very strong *M*-dependence in the allometric scaling law (as demonstrated in Mammals and Aves of Figure S6). Therefore, by defining *mtBMR* so as to minimize its *M*-dependence, we obtained a significant correlation between *mtBMR* and *STC* in contrast to a weak correlation between *msBMR* and *STC* (Table 2). The markedly large values of *mtBMR* and *STC* in Aves and Mammals strongly suggest that high degrees of dynamic conformational changes and stabilization of MMPs are realized in these animal groups, so that this stabilization effect may lower the turnover rates of mitochondria and cells, and ultimately influence organismal lifespan as well as aerobic capacity. Indeed, we obtained a significant correlation between *STC* and *MLS*, despite the enormous variations [37] in lifestyles among the different animal groups. When we recall that 10 million billion mitochondria exist in an adult human [17] and that the resources for their activation are supplied from the host cells, the stability of MMPs affecting the turnover rate of mitochondria can be a fundamental factor to sustain human life

A few animal groups of Eutheria such as rodents and insectivores (with a very high *BMR*) do not show significant *STC-HYD* and *STC-MLS* correlations [16]. These animal groups are considered to have developed a life strategy to ensure survival by countering a short longevity with quite high reproduction rates. Such behaviors in rodents and insectivores sharply contrast to those of primates with a long longevity, because a very high amino-acid replacement rate in the simian lineage is accompanied by a marked increase in *TC* and decrease in *HYD* [38]. These observations teach us that the pattern of the mt adaptive evolution is not unique even among vertebrates.

## STC describes the vertebrate behavior better than TC

The potential penalties for introducing polar residues into hydrophobic membrane proteins may explain the fact that a strong inverse correlation between *HYD* and *TC* was observed across all metazoans in this study and indeed was stronger than the correlation between *HYD* and *STC*. In contrast, in our earlier studies on primates [38] and vertebrates [16], we observed strong inverse correlations between *HYD* and *STC*. The weaker correlation reported here could relate to 2 facts: the Ser residue is more polar than the Thr residue and hence is more difficult to incorporate into very hydrophobic proteins, and the hydrophobicity of MMPs is much greater in basal metazoans such as sponges and nematodes than in vertebrates. Thus it might be relatively easy to substitute Thr residues (compared with Ser) into the MMPs of basal metazoans. This interpretation is supported by the fact that substitutions of polar residues are the most common disease-causing mutations in membrane proteins, in part through altering bilayer partitioning, but also by altering function [39]. Presumably, the more hydrophobic the membrane protein, the more problems are caused by substitution of polar residues. Conversely, the less hydrophobic the protein, the less problematic is the insertion of more polar residues such as Ser. Accordingly, we note that Ser enrichment becomes more marked in the less hydrophobic MMPs of vertebrates.

## Overall comments about the results

Thus, overall, our findings are consistent with the hypothesis that cooperative networks of hydrogen bonds involving Thr and Ser residues stabilize dynamic conformational changes in MMPs, presumably increasing aerobic capacity, although we have not measured that directly. Direct measurements of the effect of increased *TC* or *STC* on MMP catalytic efficiency (Kcat), either *in vitro* or *in vivo*, are very difficult, as each substitution is likely to be highly dependent on the context. Cryptic epistasis is common in molecular evolution [40], and the requirement for multiple interactions with nuclear as well as mitochondrial genes [41], [42] only makes the problem more extreme in the case of respiratory proteins. Moreover, respiratory flux can be increased by adaptations throughout the entire supply network, including lung structure, hemoglobin kinetics, and capillary density [43], [44], as well as substrate channeling via respirasome assembly [45]. Given this complexity, the pervasive correlation between *TC* (*STC*) and *HYD* in MMPs right across metazoans stands as strong evidence that selection for aerobic capacity at the level of mitochondrial-encoded subunits has indeed taken place. This view is consistent with a number of studies indicating regular selective sweeps on mitochondrial genes: mtDNA is far from the neutral marker it was long held to be [46].

## Remaining problems

It was difficult to detect the species-to-species coincidence between the sequence data and the observed data on *BMR* and/or *MLS*. Therefore, we used the average values of these data in respective animal groups without taking account of this coincidence. More available data in future will provide a clearer relationship between the MMP variables and *mtBMR*/*MLS* in more animal groups. We did not perform temperature adjustments of metabolic rates. One reason is that a common measurement temperature does not exist because endothermic groups do not live at body temperatures of 25°C as in many other animal groups.

Another reason is that metabolic rate and temperature are not independent variables with each other, but may be rather correlated.

## Conclusion

The deuterostome lineage presented a quite unique evolutionary pathway of a marked decrease in *HYD* and increase in *STC*, in sharp contrast with the pathway of many other animal groups showing a gradual increase in *HYD* and decrease in *STC*, reflecting the natural selection to utilize the multicellular effect. These decreases in *HYD* and increases in *STC* were remarkable in the 5 large subunits (ND4, ND5, ND2, CO1 and CO3) in complexes I and IV, which require their dynamic conformational changes to exert a high degree of proton-pumping function. The low *HYD* values for these subunits are congruent with the large *mtBMR* values associated with their dynamic mobility. Furthermore, the marked increase in *STC* can strengthen dynamic stability of them via helix-helix interactions. As a result, this dynamic stability can lower the turnover rate of mitochondria and cells, and ultimately prolong the lifespan of organisms. In this way, vertebrates (especially Aves and Mammals) are considered to have equipped an excellent mechanism of action in MMPs to attain both very high metabolic rate and long longevity.

## Supporting Information

**Figure S1 Global relationship between *TC* and *HYD* in MMPs throughout metazoans.** Strong correlations with ($R^2$> 0.9) were obtained by analyzing all 13 proteins with S>0 (see Materials and Methods).
(TIF)

**Figure S2 The *TSN*–dependence of the animal groups in various protein sets.** This figure shows that the relative positions of the 13 animal groups are invariant in any protein sets of **1**) 3-protein set (ND4, ND5, ND2), **2**) 4-protein set (ND4, ND5, ND2, ND1), **3**) 5-protein set (ND4, ND5, ND2, CO1, CO3), **4**) 6-protein set (ND4, ND5, ND2, CO1, CO3, ND1), and **5**) 7-protein set (ND4, ND5, ND2, CO1, CO3, ND1, CYTB).
(TIF)

**Figure S3 The *F*-value dependence of correlation ($R^2$) between *STC* and *mtBMR*.** The correlation ($R^2$) between *STC* and *mtBMR* is estimated by changing the *F*-value included in this quantity from 1.0 to infinity (Materials and Methods). Here, $F=\infty$ excludes the *M*-dependence of *mtBMR* completely, and *mtBMR* depends on only the constant C in each animal group.
(TIF)

**Figure S4 Neighbor-joining tree in terms of *TC* and *TSN*.** We defined the pairwise distance between the i-th and j-th animal groups by $D(i, j) = \{TC(i)-TC(j)\}^{**2}/\sigma_{TC}^{**2} + \{TSN(i)-TSN(j)\}^{**2}/\sigma_{TSN}^{**2}$. $TC(i)$ and $TSN(i)$ denote the average values of *TC* and *TSN* in the i-th animal group, respectively, by using the 5-protein set (ND4, ND5, ND2, CO1, and CO3). $\sigma_{TC}$ and $\sigma_{TSN}$ denote the standard deviations of *TC* and *TSN*, respectively.
(TIF)

**Figure S5 Two dimensional display of a tree prepared by a multidimensional vector space method.** According to the multidimensional vector space (MVS) method for preparation of a phylogenetic tree [19], the molecular evolution of a tree branch is described as going into a new dimensional space, the direction of which is therefore perpendicular to that of the original pathway. For simplicity, let us consider a tree structure in 2-dimensional (X-Y) space, as illustrated in this figure. Here, the lineage **A** represents the main pathway from the tree root to species α, and the lineage B represents a branch pattern from the lineage **A** toward species β. When X and Y are variables independent from each other without any attractions (convergent evolution), the angle between the 2 lineages is 90° (when they are closely correlated, the angle may be much deviated from 90°, as seen in the case of lines **B** and **C** of Figure 1 for the *HYD-TC/STC* strong correlation). The other species except for **A**, **B** and tree root must lie on the line **A** or **B** because they evolve into new dimensional spaces. If there are long-branch attractions, they fluctuate around these lines, as seen in this figure. We note that the lineage C may include many species but degenerates into one point in the X-Y plane and that the variables (to be used) must identify as many species as possible so as to explicitly describe a tree structure within these variables.
(TIF)

**Figure S6 The *M*-dependence of *BMR* in Aves and Mammals.**
(TIF)

**Table S1 The accession numbers of amino acid sequences of 13 animal groups.**
(XLSX)

**Table S2 A list of *msBMR* in the7 metazoan animal groups.** The 4 quantities of *msBMR*, scaling exponent α and constant C is defined in Materials and Methods.
(XLSX)

## Acknowledgments

YK is grateful to Dr. Nick Lane (University College London) for valuable discussions and insights on mitochondrial function, and thanks Drs. Junichiro Futami (Okayama University), Keiko Udaka and Takeshi Agatsuma (Kochi Medical School) for constructive discussions.

## Author Contributions

Analyzed the data: YK MT. Wrote the paper: YK. Conceived the direction of research: YK MT. Read and approved the final manuscript: YK MT.

## References

1. Makarieva AM, Gorshkov VG, Chown BL, Reich PB, Gavrilov VM (2008) Mean mass-specific metabolic rates are strikingly similar across life's major domains: Evidence for life's metabolic optimum. Proc Natl Acad Sci USA 105: 16994–16999.
2. Porter RK, Brand MD (1995) Causes of the difference in respiration rates from mammals of different body mass. Am J Physiol 269: R1213–R1224.
3. Porter RK (2001) Allometry of mammalian cellular oxygen consumption. Cell Mol Life 58: 815–822.
4. Mourier A, Larsson NG (2011) Tracing the trail of protons through complex I of the mitochondrial respiratory chain. PLoS Biol 9(8): e1001129. doi: 10.1371.
5. Baradaran R, Berrisford JM, Minhas GS, Sazanov LA (2013) Crystal structure of the entire respiratory complex I. Nature 28: 494(7438):443–448. doi: 10.1038.
6. Efremov RG, Baradaran R, Sazanov LA (2010) The architecture of respiratory complex I. Nature 465: 441–445.
7. NCBI genome database. Available: http://www.ncbi.nlm.nih.gov/genomes/.
8. Efremov RG, Sazanov LA (2011a) Structure of the membrane domain of respiratory complex I. Nature 476: 414–420.
9. Efremov RG, Sazanov LA (2011b) Respiratory complex I: 'steam engine' of the cell? Curr Opin Struct Biol 21: 532–540.
10. Tsukihara T, Shimokata K, Katayama Y, Shimada H, Muramoto K, et al. (2003) The low-spin heme of cytochrome c oxidase as the driving element of the proton-pumping process. Proc Natl Acad Sci USA 100: 15304–09.
11. Yamashita T, Voth GA (2012) Insights into the mechanism of proton transport in cytochrome c oxidase. J Am Chem Soc 134: 1147–1152.

12. Marechal A, Meunier B, Lee D, Orengo C, Rich PR (2012) Yeast cytochrome c oxidase: A model system to study mitochondrial forms of the haem–copper oxidase superfamily. Biochim Biophys Acta 1817: 620–628.
13. Hildebrand PW, Güther S, Goede A, Forrest L, Frömmel C, et al. (2008) Hydrogen-bonding and packing features of membrane proteins: functional implications. Biophys J 94: 1945–1953.
14. Eilers M, Shekar SC, Shieh T, Smith SO, Fleming PJ (2000) Internal packing of helical membrane proteins. Proc Natl Acad Sci USA 97: 5796–5801.
15. Dawson JP, Weinger JS, Engelman DM (2002) Motifs of serine and threonine can drive association of transmembrane helices. J Mol Biol 316: 799–805.
16. Kitazoe Y, Kishino H, Hasegawa M, Matsui A, Lane N, et al. (2011) Stability of mitochondrial membrane proteins in terrestrial vertebrates predicts aerobic capacity and longevity. Genome Biol Evol 3: 1233–1244.
17. Lane N (2005) Power, Sex, Suicide: Mitochondria and the Meaning of Life. Oxford: Oxford University Press.
18. Cowan R, Whittaker RG (1990) Hydrophobicity indices for amino acid residues as determined by high-performance liquid chromatography. Pept Res 3: 75–80.
19. SOSUI WWW server: Classification and secondary structure prediction of membrane proteins. Available: hppt://bp.nuap.nagaoya-u.ac.jp/sosui/.
20. TMHMM Server v. 2.0: Prediction of transmembrane helices in proteins. Available: http://www.cbs.dtu.dk/services/TMHMM/.
21. Adoutte A, Balavoine G, Lartillot N, Lespinet O, Prud'homme B, et al. (2000) The new animal phylogeny: Reliability and implications. Proc Natl Acad Sci USA 97: 4453–4456.
22. Moosmann B, Behl C (2008) Mitochondrially encoded cysteine predicts animal lifespan. Aging Cell 7: 32–46.
23. Schindeldecker M, Stark M, Behl C, Moosmann B (2011) Differential cysteine depletion in respiratory chain complexes enables the distinction of longevity from aerobicity. Mech Ageing Dev 132: 171–179.
24. Moosmann B (2011) Respiratory chain cysteine and methionine usage indicate a causal role for thiyl radicals in aging. Exp Gerontol 46: 164–169.
25. Saitou N, Nei M (1987) The neighbor-joining method: a new method for reconstructing phylogenetic trees. Mol Biol Evol 4: 406–425,
26. Kitazoe Y, Kurihara Y, Narita Y, Okuhara Y, Tominaga A, et al. (2001) A new theory of phylogeny inference through construction of multidimensional vector space. Mol Biol Evol. 18: 812–828.
27. Kitazoe Y, Kishino H, Okabayashi T, Watabe T, Nakajima N, et al. (2005) Multidimensional vector space representation for convergent evolution and molecular phylogeny. Mol Biol Evol 22:704–715.
28. Bazin E, Glemin S, Galtier N (2006) Population size does not influence mitochondrial genetic diversity in animals. Science 312: 570–572.
29. Reyes A, Gissi C, Pesole G, Saccone C (1998) Asymmetrical directional mutation pressure in the mitochondrial genome of mammals. Mol Biol Evol 15: 957–966.
30. Schmitz J, Ohme M, Zischler H (2002) The complete mitochondrial sequence of Tarsius bancanus: evidence for an extensive nucleotide compositional plasticity of primate mitochondrial DNA. Mol Biol Evol 19: 544–553.
31. Gibson A, Gowri-Shankar V, Higgs PG, Rattray M (2005) A comprehensive analysis of mammalian mitochondrial genome base composition and improved phylogenetic methods. Mol Biol Evol 22: 251–264.
32. Jobson RW, Dehne-Garcia A, Galtier N (2010) Apparent longevity-related adaptation of mitochondrial amino acid content is due to nucleotide compositional shifts. MITOCH. 10: 540–547.
33. Suarez RK, Staples JF, Lighton JRB (1999) Turnover rates of mitochondrial respiratory chain enzymes in flying honeybees (*Apis mellifera*). J Exp Biol 284: 1–6.
34. Mathiesen C, Hägerhäll C (2002) Transmembrane topology of the NuoL, M and N subunits of NADH:quinone oxidoreductase and their homologues among membrane-bound hydrogenases and bona fide antiporters. Biochim Biophys Acta Dec 2:121–132.
35. Lane N, Martin W (2010) The energetics of genome complexity. Nature 467: 929–934.
36. Lane N (2011a) Energetics and genetics across the prokaryote-eukaryote divide. Biol Direct 6: 35.
37. Owen RJ, Alexander S, Roberto SG, Carlo GC, Ralf S, et al. (2014) Diversity of ageing across the tree of life. Nature 505: 169–174.
38. Kitazoe Y, Kishino H, Hasegawa M, Nakajima N, Thorne JL, et al. (2008) Adaptive threonine increase in transmembrane regions of mitochondrial proteins in higher primates. PLoS One. 3: e3343.
39. Joh NHJ, Min A, Faham S, Whitelegge JP, Yang D, et al. (2008) Modest stabilization by most hydrogen-bonded side-chain interactions in membrane proteins. Nature 453: 1266–1272.
40. Lunzer M, Golding GB, Dean AM (2010) Pervasive cryptic epistasis in molecular evolution. PLoS Genet 6: e1001162.
41. Lane N (2011b) Mitonuclear match: optimizing fitness and fertility over generations drives aging within generations. BioEssays 33: 860-869.
42. Lane N (2011c) The costs of breathing. Science 334: 184–5.
43. Suarez RK (1998) Oxygen and the upper limits to animal design and performance. J Exp Biol 201: 1065–1072.
44. Maina JN (2000) What it takes to fly: the structural and functional respiratory refinements in birds and bats. J Exp Biol 203: 3045–3064.
45. Acin-Perez R, Fernández-Silva P, Peleato ML, Pérez-Martos A, Enriquez JA (2008) Respiratory active mitochondrial supercomplexes. Mol Cell 32: 529–539.
46. Bazin E, Glemin S, Galtier N (2006) Population size does not influence mitochondrial genetic diversity in animals. Science 312: 570–572.

Journal of the Neurological Sciences 346 (2014) 350–352

Contents lists available at ScienceDirect

Journal of the Neurological Sciences

journal homepage: www.elsevier.com/locate/jns

Letter to the editor

# Amelioration of acylcarnitine profile using bezafibrate and riboflavin in a case of adult-onset glutaric acidemia type 2 with novel mutations of the electron transfer flavoprotein dehydrogenase (*ETFDH*) gene

*Keywords:*
Glutaric acidemia type 2
Acylcarnitine profile
Adult onset
Bezafibrate

## 1. Introduction

Multiple acyl-coenzyme A dehydrogenase deficiency (MADD), also known as glutaric acidemia type 2 (GA2), was first described in 1976 [1]. GA2 is a rare autosomal recessive disorder whose biochemical abnormalities result from a deficiency of one of the two electron transfer flavoproteins (ETF and ETFDH) that transfer electrons from acyl-CoA dehydrogenases to the respiratory chain [2]. The disorder affects multiple metabolic pathways involving branched amino acids, fatty acids, and tryptophan, and results in a variety of distinctive organic acids being discharged. The heterogeneous clinical features of patients with GA2 fall into three subclasses: two neonatal-onset forms (types I/II) and a late-onset form (type III) [3]. The late-onset form is typically characterized by intermittent vomiting, hypoglycemia, hepatomegaly, metabolic acidosis, and/or hyperammonemia, symptoms that are often triggered by general infections or catabolic conditions [4].

Here, we describe the case of a man with lipid-storage myopathy, low muscle carnitine, and an adult-onset form of GA2 with two novel mutations in the *ETFDH* gene. In this case, a combination of a hypolipidemic drug (bezafibrate), riboflavin, and L-carnitine was effective in treating the disease.

## 2. Case report

A 31-year-old man was referred to our hospital because of muscle weakness and limb fatigability. Nine months earlier, he had gradually developed proximal muscle weakness and fatigability. He exhibited normal psychomotor development. His relatives had no history of neuromuscular disease. Physical examination on admission showed a normally developed, well-nourished man (185 cm, 73 kg) without hepatosplenomegaly. Neurological examination revealed mild muscle weakness in his left iliopsoas muscle (grade 5−). Muscle amyotrophy and myalgia were not noted. The following serum biochemistry markers were elevated: creatine kinase (CK), 689 U/L (normal <230); creatine kinase-MB, 50 U/L (<10); aldolase, 8.9 IU/L (<5.9); myoglobin, 107 ng/mL (<72.0); and triglycerides, 315 mg/dL (<149). The full blood count, blood glucose, renal and thyroid function, immunoglobulins, inflammatory markers, and antinuclear antibodies were normal. Echocardiography, pulmonary function tests, and a brain MRI were normal. Abdominal echography revealed only the fatty liver. A muscle MRI showed a high-density area in the bilateral lower limb muscles in short-T1 inversion recovery (STIR) (Fig. 1A). Atrophy of the biceps was suspected based on a muscle CT scan. Electromyography of the left vastus lateralis muscle and the tibialis anterior muscle displayed myopathic patterns. In the muscle biopsy specimen from the biceps brachii, neither lymphocytic infiltration nor endomysial fibrosis was observed (Fig. 1B), although some fibers contained many vacuoles. These were positively stained with Oil Red O, suggesting a lipid storage myopathy (Fig. 1C).

Total and free carnitine concentrations in muscle specimens were severely decreased at 3.5 (control 15.7 ± 2.8) and 1.7 (12.9 ± 3.7) nmol/mg non-collagen protein (NCP), respectively. Activity of acyl-CoA dehydrogenases was normal. Analysis of urinary organic acids showed increased 2-OH-glutarate, ethylmalonate, and 3-OH-propionate. The acylcarnitine profile of the patient's serum showed a broad-range elevation of acylcarnitines, but no abnormalities were observed in the amino acid profile. This indicated a multiple-dehydrogenation abnormality, which is consistent with GA2. After receiving informed consent, the patient's skin fibroblasts were isolated and cultured, as described previously [5]. Genetic analysis identified novel, compound heterozygous missense mutations in the *ETFDH* gene (890G > T/W297L and 950C > G/P317R). Western blot analysis showed decreased production of ETFDH in the patient's fibroblasts (Fig. 1D). This indicated that the mutations would be pathogenic.

Following treatment with L-carnitine alone, the patient's serum CK reached nearly normal levels. However, his serum acylcarnitine profile remained abnormal (Fig. 1E, left panel). The L-carnitine treatment was then supplemented with riboflavin at 105 mg/day or with bezafibrate (BEZ; 600 mg/day) because the patient showed mild hyperlipidemia, and because this hypolipidemic drug was effective for adolescent GA2 patients [5]. However, the combined treatment of L-carnitine and riboflavin, or L-carnitine and BEZ, failed to improve the acylcarnitine profile (Fig. 1E, left panel) and the patient's symptoms remained stable. For the next 7 months, the patient was treated with L-carnitine alone. During this period, he felt fatigability and his serum CK increased mildly. BEZ was again added to his treatment regimen. His serum acylcarnitine profile improved, but his serum CK remained high and he occasionally complained of fatigue (Fig. 1E, right panel). After 15 months, riboflavin was added to the L-carnitine and BEZ. His serum CK and acylcarnitine profile returned to normal within one month, and his symptoms completely disappeared. This amelioration has continued beyond 6 months.

## 3. Discussion

We diagnosed a patient with GA2 based on observations of the muscle pathology, acylcarnitine analysis, and *ETFDH* gene mutations. In the

http://dx.doi.org/10.1016/j.jns.2014.08.040

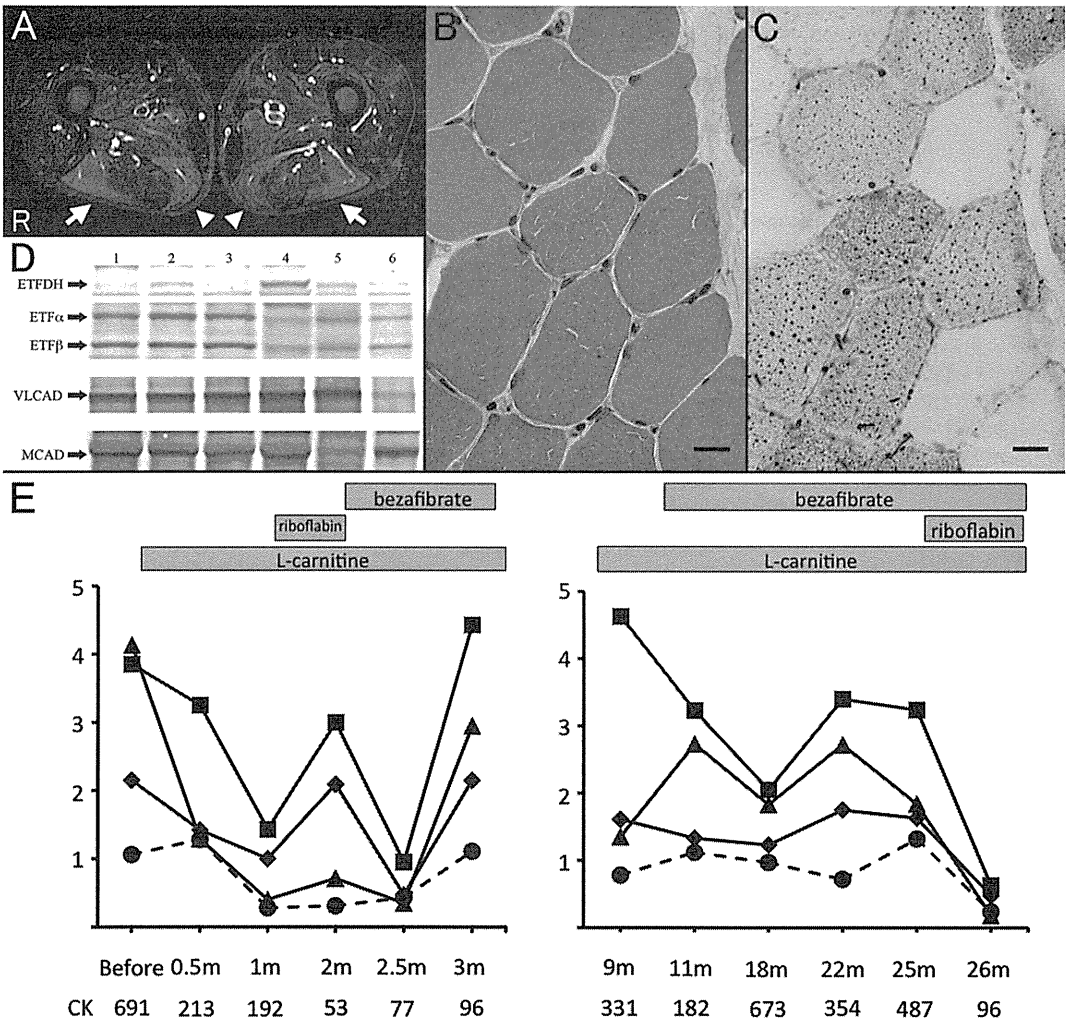


**Fig. 1.** A. A muscle MRI showed an area of high intensity in the bilateral biceps femoris muscle (arrow) and semimembranous muscle (arrowheads) in short-T1 inversion recovery (STIR). This indicated that increased water content in these muscles due to cellular lysis or fluid accumulation secondary to inflammation [10]. B, C. Biopsy of the patient's right biceps muscle. (B) Hematoxylin and eosin staining showed multiple optically empty vacuoles. (C) Oil Red O staining revealed excessive lipid droplets. The scale bar represents 20 μm. D. Western blot analyses of proteins in the patient's fibroblasts. The patient's fibroblasts were prepared as described previously [5,11]. For analysis of ETFDH, ETFα, and ETFβ, 25 μg of protein was applied to the gel. For analysis of very long-chain acyl-CoA dehydrogenase (VLCAD) and medium-chain acyl-CoA dehydrogenase (MCAD), 10 μg of protein was applied to the gel. Lane 1, patient's fibroblasts; lane 2, control (normal) fibroblasts; lane 3, ETFDH-defective fibroblasts; lane 4, ETFβ-defective fibroblasts; lane 5, MCAD-defective fibroblasts; lane 6, VLCAD-defective fibroblasts. Note that lane 1 from this patient, and lane 3 from the negative control, lack the band corresponding to ETFDH. This indicates that this patient had no ETFDH protein. Compared to control, the patient's fibroblasts showed no change in the expression of ETFα, ETFβ, VLCAD, or MCAD proteins. E. Changes in blood acylcarnitines with various treatments. The acylcarnitine profile of the patient's serum before treatment showed a broad-range elevation of acylcarnitines, including C6, C8, C10, C12, C14, and C16 acylcarnitine at 1.06 nmol/mL (normal <0.46), 2.15 (<1), 3.84 (<0.8), 4.13 (<0.4), 2.81 (<0.3), and 2.22 (<0.5), respectively. In the left panel, BEZ or riboflavin combined with L-carnitine, partially improved serum CK and serum acylcarnitine levels. Combining all three agents completely restored to normal the patient's acylcarnitine profile (right panel). During the seven-month period between the results shown in panels E and F, the patient was treated with L-carnitine alone. Units for acylcarnitine are nmol/mL and for CK are U/L. "m" indicates month. ●, C4; ◆, C8; ■, C10; ▲, C12.

adult myopathic form of GA2, patients sometimes do not show rhabdomyolysis, and there is no typical biochemical examination that can help us to consider the presence of a fatty acid oxidation disorder (FAO), as was observed here. Muscle biopsy and acylcarnitine analysis provide useful information and should be employed without hesitation.

Intake of L-carnitine has been reported to either exacerbate symptoms or to be effective for GA2 patients [6,7]. In the present case, oral carnitine alone leads to only partial improvement based on amelioration of the patient's muscle weakness and decreases in his serum CK and acyl-CoA. Riboflavin supplementation produces improvements in the symptoms and metabolic profiles of GA2 patients with *ETFDH* mutations, and the late-onset form [2]. BEZ is a hypolipidemic drug that is as an agonist of the peroxisome proliferating activator receptor, and was found to be beneficial in Japanese children with *ETFDH* gene mutations exhibiting GA2 [5]. Several mechanisms for the effectiveness of BEZ for FAO have been reported including upregulating mRNA and the activity of several FAO enzymes [8,9]. In the present case, BEZ, L-carnitine, and riboflavin each showed partial effectiveness and produced partial remission in a patient with GA2. In children, BEZ has been administered at doses from 17 to 25 mg/kg/day [5]. In the current patient, 600 mg/day of BEZ was administered, corresponding to only 8.2 mg/kg/day. This low dose was used because of the limitations of BEZ as a hypolipidemic drug and may explain the limited effectiveness of BEZ for our patient. A combination of BEZ, riboflavin, and L-carnitine produced complete remission in this patient, not only of his symptoms and serum CK, but also of his defect in fatty acid metabolism.

This case supports a new option for the treatment of GA2 patients, even in adults. Additional clinical studies and experimental investigation of the mechanisms of action of these drugs are required.

## Conflict of interest

The authors have no conflicts of interest to declare.

## References

[1] Przyrembel H, Wendel U, Becker K, Bremer HJ, Bruinvis L, Ketting D, et al. Glutaric aciduria type II: report on a previously undescribed metabolic disorder. Clin Chim Acta 1976;66:227–39.
[2] Liang WC, Nishino I. Lipid storage myopathy. Curr Neurol Neurosci Rep 2011;11: 97–103.
[3] Olsen RKJ, Andresen BS, Christensen E, Bross P, Skovby F, Gregersen N. Clear relationship between ETF/ETFDH genotype and phenotype in patients with multiple acyl-CoA dehydrogenation deficiency. Hum Mutat 2003;22:12–23.
[4] Yotsumoto Y, Hasegawa Y, Fukuda S, Kobayashi H, Endo M, Fukao T, et al. Clinical and molecular investigations of Japanese cases of glutaric acidemia type 2. Mol Genet Metab 2008;94:61–7.
[5] Yamaguchi S, Li H, Purevsuren J, Yamada K, Furui M, Takahashi T, et al. Bezafibrate can be a new treatment option for mitochondrial fatty acid oxidation disorders: evaluation by in vitro probe acylcarnitine assay. Mol Genet Metab 2012;107:87–91.
[6] Green A, Preece MA, De Sousa C, Pollitt RJ. Possible deleterious effect of L-carnitine supplementation in a patient with mild multiple acyl-CoA dehydrogenation deficiency (ethylmalonic-adipic aciduria). J Inherit Metab Dis 1991;14:691–7.
[7] Donato SD, Frerman FE, Rimoldi M, Rinaldo P, Taroni F, Wiesmann UN. Systemic carnitine deficiency due to lack of electron transfer flavoprotein: ubiquinone oxidoreductase. Neurology 1986;36:957–63.
[8] Bonnefont JPJ, Bastin JJ, Laforêt PP, Aubey FF, Mogenet AA, Romano SS, et al. Long-term follow-up of bezafibrate treatment in patients with the myopathic form of carnitine palmitoyltransferase 2 deficiency. Clin Pharmacol Ther 2010; 88:101–8.
[9] Djouadi F. Bezafibrate increases very-long-chain acyl-CoA dehydrogenase protein and mRNA expression in deficient fibroblasts and is a potential therapy for fatty acid oxidation disorders. Hum Mol Genet 2005;14:2695–703.
[10] Diekman EF, van der Pol WL, Nievelstein RAJ, Houten SM, Wijburg FA, Visser G. Muscle MRI in patients with long-chain fatty acid oxidation disorders. J Inherit Metab Dis 2013;37:405–13.
[11] Endo M, Hasegawa Y, Fukuda S, Kobayashi H, Yotsumoto Y, Mushimoto Y, et al. In vitro probe acylcarnitine profiling assay using cultured fibroblasts and electrospray ionization tandem mass spectrometry predicts severity of patients with glutaric aciduria type 2. J Chromatogr B 2010;878:1673–6.

Ayako Shioya
Hiroshi Takuma*
*Department of Neurology, Faculty of Medicine, University of Tsukuba, Ibaraki, Japan*
*Corresponding author at: 1-1-1 Tennodai, Tsukuba, Ibaraki, 305-8575, Japan. Tel./fax: +81 29 853 3224.
*E-mail address:* htakuma@md.tsukuba.ac.jp (H. Takuma).

Seiji Yamaguchi
*Department of Pediatrics, Shimane University School of Medicine, Shimane, Japan*

Akiko Ishii
*Department of Neurology, Faculty of Medicine, University of Tsukuba, Ibaraki, Japan*

Masahiko Hiroki
*Department of Neurology, Tsukuba Medical Center Hospital, Ibaraki, Japan*

Tokiko Fukuda
*Department of Pediatrics, Hamamatsu University School of Medicine, Shizuoka, Japan*

Hideo Sugie
*Department of Pediatrics, Jichi Medical University, Tochigi, Japan*

Yosuke Shigematsu
*Department of Health Science, University of Fukui, Fukui, Japan*

Akira Tamaoka
*Department of Neurology, Faculty of Medicine, University of Tsukuba, Ibaraki, Japan*

24 June 2014

RESEARCH ARTICLE

Human Mutation

OFFICIAL JOURNAL
HGVS
HUMAN GENOME VARIATION SOCIETY
www.hgvs.org

# ECHS1 Mutations Cause Combined Respiratory Chain Deficiency Resulting in Leigh Syndrome

Chika Sakai,[1] Seiji Yamaguchi,[2] Masayuki Sasaki,[3] Yusaku Miyamoto,[4] Yuichi Matsushima,[1,5]* and Yu-ichi Goto[1]*

[1]*Department of Mental Retardation and Birth Defect Research, National Institute of Neuroscience, National Center of Neurology and Psychiatry, Kodaira, Tokyo, Japan;* [2]*Department of Pediatrics, Shimane University, Izumo, Shimane, Japan;* [3]*Department of Child Neurology, National Center Hospital, National Center of Neurology and Psychiatry, Kodaira, Tokyo, Japan;* [4]*Department of Pediatrics, St. Marianna University School of Medicine, Kawasaki, Kanagawa, Japan;* [5]*Department of Clinical Chemistry and Laboratory Medicine, Graduate School of Medical Sciences, Kyushu University, Fukuoka, Japan*

Communicated by David Rosenblatt

Received 4 September 2014; accepted revised manuscript 5 November 2014.
Published online 13 November 2014 in Wiley Online Library (www.wiley.com/humanmutation). DOI: 10.1002/humu.22730

**ABSTRACT:** The human *ECHS1* gene encodes the short-chain enoyl coenzyme A hydratase, the enzyme that catalyzes the second step of β-oxidation of fatty acids in the mitochondrial matrix. We report on a boy with ECHS1 deficiency who was diagnosed with Leigh syndrome at 21 months of age. The patient presented with hypotonia, metabolic acidosis, and developmental delay. A combined respiratory chain deficiency was also observed. Targeted exome sequencing of 776 mitochondria-associated genes encoded by nuclear DNA identified compound heterozygous mutations in *ECHS1*. ECHS1 protein expression was severely depleted in the patient's skeletal muscle and patient-derived myoblasts; a marked decrease in enzyme activity was also evident in patient-derived myoblasts. Immortalized patient-derived myoblasts that expressed exogenous wild-type ECHS1 exhibited the recovery of the ECHS1 activity, indicating that the gene defect was pathogenic. Mitochondrial respiratory complex activity was also mostly restored in these cells, suggesting that there was an unidentified link between deficiency of ECHS1 and respiratory chain. Here, we describe the patient with ECHS1 deficiency; these findings will advance our understanding not only the pathology of mitochondrial fatty acid β-oxidation disorders, but also the regulation of mitochondrial metabolism.
Hum Mutat 36:232–239, 2015. © 2014 Wiley Periodicals, Inc.

**KEY WORDS:** combined respiratory chain deficiency; Leigh syndrome; ECHS1; fatty acid β-oxidation disorder

## Introduction

Mitochondrial fatty acid β-oxidation provides carbon substrates for gluconeogenesis during the fasting state and contributes electrons to the respiratory chain for energy production. Once a fatty acid is activated to the acyl-coenzyme A (CoA) form and enters the mitochondrial fatty acid β-oxidation pathway, it undergoes the four following enzymatically catalyzed reaction steps during each β-oxidation cycle (Supp. Table S1): (1) dehydrogenation, (2) hydration, (3) a second dehydrogenation step, and finally (4) a thiolytic cleavage that generates one acetyl-CoA or, in certain cases, one propionyl-CoA and an acyl-CoA that is two carbons shorter than the acyl-CoA precursor. Each individual step involves specific enzymes encoded by different genes with different substrate preferences (Supp. Table S1). The first dehydrogenation reaction is catalyzed mainly by four enzymes—short-, medium-, long-, and very long chain acyl-CoA dehydrogenases (SCAD, MCAD, LCAD, and VLCAD)—with substrate optima of C4, C8, C12, and C16 acyl-CoA esters, respectively, still each dehydrogenase can utilize other suboptimal substrates [Ikeda et al., 1983, 1985a, 1985b; Ensenauer et al., 2005]. The short-chain enoyl-CoA hydratase (ECHS1) catalyzes the next step and has substrate optima of C4 2-trans-enoyl-CoA, also called crotonyl-CoA. Although ECHS1 also catalyzes hydration of medium chain substrates, longer acyl chains (e.g., C16-intermediates) are hydrated by mitochondrial trifunctional protein (MTP) [Uchida et al., 1992; Kamijo et al., 1993]. MTP consists of an alpha-subunit with long-chain enoyl-CoA hydratase and long-chain 3-hydroxyacyl-CoA dehydrogenase (LCHAD) activities and a beta-subunit with long-chain 3-ketothiolase activity.

Mitochondrial fatty acid β-oxidation disorders generally cause impaired energy production and accumulation of partially oxidized fatty acid metabolites. They are clinically characterized by hypoglycemic seizures, hypotonia, cardiomyopathy, metabolic acidosis, and liver dysfunction [Kompare and Rizzo, 2008]. The most common genetic defect in MTP is LCHAD deficiency [MIM #609016]; deficiency involving reduced activity of all three MTP enzymes [MIM #609015] is reported much less frequently and is often associated with infantile mortality secondary to severe cardiomyopathy [Spiekerkoetter et al., 2004]. Deficiency of SCAD [MIM #201470], which catalyzes the first dehydrogenation reaction and has similar substrate optima with regard to carbon chain as ECHS1, have been studied for years, and the range of associated phenotypes includes failure to thrive, metabolic acidosis, ketotic hypoglycemia, developmental delay, seizures, and neuromuscular symptoms such as myopathy and hypotonia [Jethva et al., 2008].

Additional Supporting Information may be found in the online version of this article.

*Correspondence to: Yu-ichi Goto. Department of Mental Retardation and Birth Defect Research, National Institute of Neuroscience, National Center of Neurology and Psychiatry, Kodaira, Tokyo, 187-8502, Japan. E-mail: goto@ncnp.go.jp; Yuichi Matsushima. Department of Clinical Chemistry and Laboratory Medicine, Graduate School of Medical Sciences, Kyushu University, Fukuoka, Fukuoka, 812-8582, Japan. E-mail: matsush5@cclm.med.kyushu-u.ac.jp

Contract grant sponsor(s): Grants-in-Aid for Research on Intractable Diseases (Mitochondrial Disease) from the Ministry of Health, Labor and welfare of Japan; Research Grant for Nervous and Mental Disorders from the National Center of Neurology and Psychiatry (21A-6, 24-8) and JSPS KAKENHI (25670275).

Here, we describe a patient with ECHS1 deficiency who presented with Leigh syndrome [MIM #256000] accompanied by hypotonia, metabolic acidosis, and developmental delay. Additionally, the patient presented with combined respiratory chain deficiency, which is not commonly described in most clinical reports of mitochondrial fatty acid $\beta$-oxidation disorders. Finally, we discuss the pathology of ECHS1 deficiency and possible interactions between mitochondrial fatty acid $\beta$-oxidation and the respiratory chain, which are two important pathways in mitochondrial energy metabolism.

## Materials and Methods

This study was approved by the ethical committee of National Center of Neurology and Psychiatry. All the samples in this study were taken and used with informed consent from the family.

### Whole-mtDNA Genome Sequence Analysis

Long and accurate PCR amplification of mtDNA followed by direct sequencing was performed according to the previous publication with a slight modification [Matsunaga et al., 2005].

### Targeted Exome Sequencing

Almost all exonic regions of 776 nuclear genes (Supp. Table S2), in total 7,368 regions, were sequenced using the Target Enrichment System for next-generation sequencing (HaloPlex; Agilent Technologies, Santa Clara, California, USA) and MiSeq platform (Illumina, San Diego, California, USA). Sequence read alignment was performed with a Burrows–Wheeler Aligner (version 0.6.1) to the human reference genome (version hg19). Realignment and recalibration of base quality scores was performed with the Genome Analysis Toolkit (version 1.6.13). Variants were detected and annotated against dbSNP 135 and 1000 Genomes data (February 2012 release) by Quickannotator.

### Sanger Sequencing

Sanger sequencing of candidate genes was performed with the BigDye Terminators v1.1 Cycle Sequencing kit (Thermo Fisher Scientific, Waltham, Massachusetts, USA) as per manufacturer's protocol. Details of primers and conditions are available upon request. DNA sequences from the patients were compared against the RefSeq sequence and the sequences of a healthy control or parents those were sequenced in parallel.

### Cell Culture

The patient-derived primary myoblasts were established from the biopsy of patient's skeletal muscle and cultured in DMEM/F-12 (Thermo Fisher Scientific) supplemented with 20% (v/v) heat-inactivated fetal bovine serum (FBS, Thermo Fisher Scientific). DLD-1 (human colon carcinoma) cells were provided by Taiho pharmaceutical company (Tokyo, Japan) and cells were cultured in RPMI-1640 (Thermo Fisher Scientific) supplemented with 10% (v/v) heat-inactivated FBS (Thermo Fisher Scientific). All cells were cultured in 5% $CO_2$ at 37°C.

### Preparation of Mitochondrial Fraction

Mitochondrial fractions from patient's skeletal muscle and patient-derived myoblasts were prepared according to the literature with a slight modification [Frezza et al., 2007].

### Immunoblotting

Mitochondrial fraction and protein lysates were prepared from patient's skeletal muscle and patient-derived Myoblasts. Thirty micrograms of protein of mitochondrial fraction or 50 micrograms of protein lysate was separated on 4%–12% Bis-Tris gradient gels (Thermo Fisher Scientific) and transferred to polyvinylidene fluoride membranes. Primary antibodies used were against ECHS1 (Sigma-Aldrich, St. Louis, Missouri, USA), complex II 70 kDa subunit (Abcam, Cambridge, England), $\beta$-actin (Santa Cruz, Biotechnology, Dallas, Texas, USA), HA (Wako, Tokyo, Japan), and AcGFP (Thermo Fisher Scientific).

### Enzyme Assays

Enzyme activities of mitochondrial respiratory complexes I–V and citrate synthase (CS) were measured in mitochondrial fraction prepared from patient's specimens. The assays for complexes I–IV and CS were performed as described previously [Shimazaki et al., 2012]. The assay for complex V was carried out following the method by Morava and his colleagues with modifications [Morava et al., 2006]. The enoyl-CoA hydratase activity was assayed by the hydration of crotonyl-CoA by a slight modification of the procedure described earlier [Steinman and Hill, 1975]. Five micrograms of protein of the mitochondrial fraction prepared from patient-derived myoblasts was added to 0.3 M Tris–HC1, pH 7.4, containing 5 mM EDTA (Ethylenediaminetetraacetic acid). The reaction was started by the addition of 200 $\mu$M crotonyl-CoA and the decrease in absorbance at 280 nm was monitored at 30°C.

### Construction of the Immortalized Patient-Derived Myoblasts

The patient-derived myoblasts and control myoblasts were transfected with pEF321-T vector (A kind gift from Dr. Sumio Sugano, University of Tokyo) and the cells were cultured serially for more than ten population doublings until the morphological alteration was observed [Kim et al., 1990].

### Expression Vector Preparation and Transfection

For construction of a mammalian expression vector, full-length *ECHS1* (GenBank accession number NM_004092.3) was amplified from a cDNA prepared from control subject using PrimeSTAR GXL DNA polymerase (TaKaRa, Tokyo, Japan). The PCR product was cloned into pEBMulti-Pur (Wako) and the clone was verified by Sanger sequencing. The empty expression vector or an ECHS1 expression vector was transfected into immortalized patient-derived myoblasts using Lipofectamine LTX Reagent (Thermo Fisher Scientific). Each of the two missense variants, c.2T>G; p.M1R and c.5C>T; p.A2V, was independently introduced into the clone by PCR-based site-directed mutagenesis. Each insert with C-terminal HA tag was cloned into pIRES2-AcGFP1 (Clontech Laboratories, Mountain View, California, USA) and the clones were verified by Sanger sequencing. WT and mutant ECHS1 expression vector were transfected into DLD-1 cells using Lipofectamine LTX Reagent (Thermo Fisher Scientific). Twenty-four hours later, the cell lysate was subjected to immunoblotting.

## Results

The patient reported here was a boy born to unrelated, healthy parents after a 40-week pregnancy (weight 3,300 g, length 52 cm,

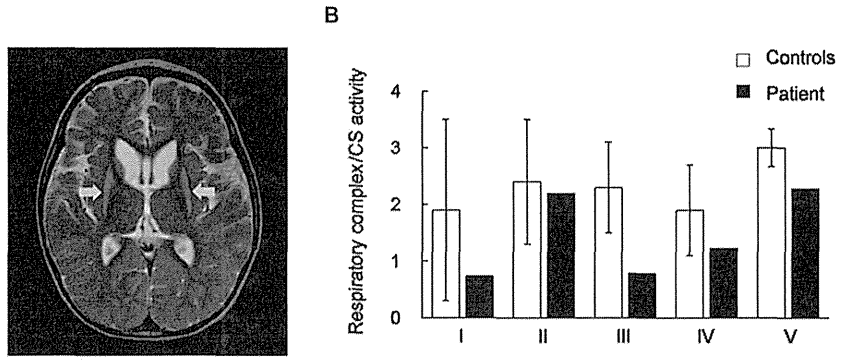


**Figure 1.** T2-weighted magnetic resonance scan image and enzyme activities of mitochondrial respiratory complexes. **A**: T2-weighted magnetic resonance scan image (MRI) shows bilaterally symmetrical hyperintensities in the putamen (arrows in the image); these are characteristic of Leigh syndrome. **B**: Enzymatic activities of five mitochondrial respiratory complexes (I, II, III, IV, and V) were measured in mitochondrial fractions prepared from the patient's skeletal muscle. Respiratory complexes activities were normalized to citrate synthase activity. Black bars show patient values and white bars show control values. Control values were mean values obtained from five healthy individuals. Patient activity values for complexes I, III, and IV were 39%, 34%, and 64% of the control values, respectively. Error bars represent standard deviations.

**Table 1. Urinary Organic Acid Profiling**

| | Patient RPA (%) | Controls RPA (%) |
|---|---|---|
| TCA cycle intermediates | | |
| α-Ketoglutarate | 4.52 | 3.00–102.90 |
| Aconitate | 20.37 | 15.10–86.10 |
| Isocitrate | 8.98 | 8.30–29.00 |
| Other metabolites | | |
| Lactate | 11.83[a] | <4.70 |
| Pyruvate | 3.18 | <24.10 |
| 3-Hydroxyisobutyric acid | 1.95 | <9.00 |
| Methylcitric acid | 0.14[a] | Less than trace amount |
| *p*-Hydroxy-phenyllactic acid | 40.05[a] | <7.00 |
| Glyoxylate | 37.71[a] | <6.10 |

[a]Values outside the normal range.
RPA(%), relative peak area to the area of internal standard (heptadecanoic acid, HDA).

occipitofrontal circumference (OFC) 34.5 cm). Auditory screening test at 2 months of age revealed hearing impairment, and he began to use a hearing aid at 6 months of age. Psychomotor developmental delay was noted at 5 months of age; he could not sit alone, or speak a meaningful word as of 4 years of age. Nystagmus was noted at 10 months of age. Muscle hypotonia, spasticity, and athetotic trunk movement became prominent after 1 year of age. His plasma (20.2 mg/dl) and a cerebrospinal fluid lactate were elevated (25.3 mg/dl, control below 15 mg/dl). Urinary organic acid profiling reveals significantly elevated excretion of glyoxylate (Table 1). Analysis of blood acylcarnitines showed no abnormalities. Brain magnetic resonance scan image showed bilateral T2 hyperintensity of the putamen, typical for Leigh syndrome (Fig. 1A). Because Leigh syndrome is generally caused by defects in the mitochondrial respiratory chain or the pyruvate dehydrogenase complex, we performed a muscle biopsy to measure enzyme activities of mitochondrial respiratory complexes in the patient. Mitochondrial fractions prepared from patient or control specimens were used for all activity measurements. Activity of each respiratory complex was normalized relative to CS activity; normalized values for complexes I, III, and IV activity were decreased to 39%, 34%, and 64% of control values, respectively (Fig. 1B). Moreover, we performed blue native PAGE (BN-PAGE) to examine if the assembly of respiratory complexes were altered in the patient. As a result, there were no clear difference between the patient and the control (Supp. Fig. S1).

Mitochondrial respiratory chain defects can be due to pathogenic mutations in mitochondrial DNA (mtDNA) or nuclear DNA (nDNA) coding for mitochondrial components. Initially, long and accurate PCR amplification of mtDNA followed by direct sequencing was performed and no mutations known to be associated with Leigh syndrome were identified, but previously reported polymorphisms were found (Supp. Table S3). Therefore, to identify the responsible mutations in nDNA, targeted exome sequencing was performed. Coverage was at least 10× for 86.2% of the target regions, and 30× or more for 73.4%. In all, 5,640 potential variants were identified; these included 811 splice-site or nonsynonymous variants. Among those 811 variants, 562 were on the mismapping reads that contained multiple apparent mismatches to the reference DNA sequence. Of the remaining 249 variants, nine that were on target regions with less than 10× coverage were eliminated because data reliability was low. Filtering against dbSNP 135 and 1000 Genomes data, this number was reduced to 13 including compound heterozygous variants in the *ECHS1* [MIM #602292] and 11 heterozygous variants in 11 separate genes (Supp. Table S4). Those variants have been submitted to dbSNP (http://www.ncbi.nlm.nih.gov/SNP/). Because most mitochondrial diseases caused by known nDNA mutations are inherited in an autosomal recessive manner, we focused on the compound heterozygous variants in *ECHS1*—c.2T>G; p.M1R and c.5C>T; p.A2V—as primary candidates.

To confirm the targeted exome sequencing results, we performed Sanger sequencing of genomic *ECHS1* DNA and *ECHS1* cDNA from the patient and his parents. We identified both variants, c.2T>G and c.5C>T, and the respective normal alleles in genomic DNA and cDNA from the patient (Fig. 2A and B) and no other *ECHS1* variants were detected except for common SNPs in the open reading frame. Analysis of genomic DNA from the patient's parents showed that patient's father was heterozygous for only one variant, c.2T>G, and the patient's mother for only the other variant, c.5C>T (Fig. 2A). These results indicated that the patient inherited each variant separately and that both mutant alleles were expressed in the patient (Fig. 2B). Each variant was nonsynonymous and in the region encoding the mitochondrial transit peptide (1–27 amino acids) of ECHS1 [Hochstrasser et al., 1992]; moreover, c.2T>G; p.M1R was a start codon variant (Fig. 2C).

Next, immunoblotting with primary antibodies against ECHS1 was performed to assess protein expression. Mitochondrial

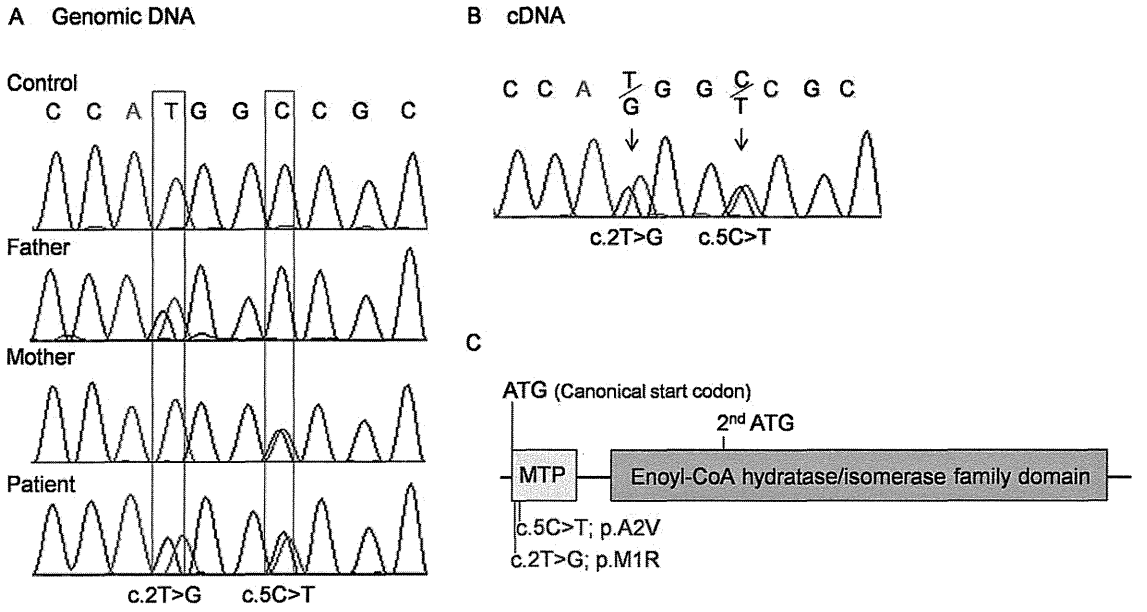


**Figure 2.** *ECHS1* Sanger sequencing analysis and ECHS1 functional domains. **A**: Sequence chromatograms from part of exon 1 of *ECHS1* were generated by Sanger sequencing of genomic DNA. Each parent had one wild-type allele; the patient's father also harbored a c.2T>G variant, and the patient's mother a c.5C>T variant. The patient inherited each variant allele and was a compound heterozygote. **B**: Sequence chromatograms from part of *ECHS1* exon 1 obtained by Sanger sequencing of cDNA prepared from patient mRNA. The same variants seen in genomic DNA were observed in the cDNA. **C**: A schematic diagram of the functional domains in ECHS1 and the locations of the mutations. MTP, mitochondrial transit peptide.

fractions prepared from patient and control skeletal muscle were used; whole-cell lysates or mitochondrial fractions prepared from patient-derived or control myoblasts were also used. All experiments using these specimens showed that the expression level of ECHS1 protein of the patient was too low to detect by immunoblotting even though the expression level of SDHA was almost the same as controls (Fig. 3A–C). These findings indicated that c.2T>G; p.M1R and c.5C>T; p.A2V mutations caused a remarkable reduction in ECHS1 protein expression. Notably, patient-derived and control myoblasts were similar with regard to *ECHS1* mRNA expression (Fig. 3D), indicating that the mutations apparently affected ECHS1 protein expression directly. Next, we measured ECHS1 enzyme activity in mitochondrial fractions prepared from patient-derived and control myoblasts. ECHS1 activity was normalized to CS activity, and activity in patient-derived myoblasts was 13% of that in control myoblasts (Fig. 3E). Therefore, the mutations caused a severe depletion of ECHS1 protein expression thereby decreasing ECHS1 enzyme activity.

To examine the stability of each mutated protein, we constructed three pIRES2-AcGFP1 expression plasmids, each expressed a different HA-tagged protein: wild-type, M1R-mutant, or A2V-mutant ECHS1. The expression of AcGFP was used as a transfection control. After the transfection into DLD-1 cells, immunoblotting of whole-cell lysate with anti-HA and GFP antibodies showed markedly higher expression of wild-type ECHS1 than of either mutant protein; all ECHS1 expression was normalized to AcGFP expression (Fig. 4, Supp. Fig. S2). This result indicated that ECHS1 protein expression was significantly reduced in the patient because of each mutation.

To confirm that the patient had ECHS1 deficiency, we performed a cellular complementation experiment. Patient-derived myoblasts had to be immortalized for these experiments because nonimmortalized cells exhibited poor growth and finite proliferation. The patient-derived myoblasts and control myoblasts were transfected with pEF321-T vector (a kind gift from Dr. Sumio Sugano, University of Tokyo). We then ascertained that ECHS1 protein expression and activity were lower in immortalized patient-derived myoblasts than in controls (Fig. 5A and B). We then transduced an empty expression vector, pEBMulti-Pur (Wako), or a pEBMulti-Pur construct containing a full-length, wild-type *ECHS1* cDNA into the immortalized patient-derived myoblasts; cells with the vector only or the ECHS1-expression construct are hereafter called vector-only and rescued myoblasts, respectively. ECHS1 protein expression level and enzyme activity were analyzed in mitochondrial fractions prepared from rescued myoblasts. Relative expression level of ECHS1 in rescued myoblasts was 11 times higher than that in vector-only myoblasts (Fig. 5A), and ECHS1 activity normalized to CS activity in rescued myoblasts was 49 times higher than that in vector-only myoblasts (Fig. 5B). From these cellular complementation experiments, we concluded the patient had ECHS1 deficiency.

Since the patient showed the combined mitochondrial respiratory chain deficiency in the skeletal muscle as mentioned above, we used a cellular complementation experiment to determine whether wild-type ECHS1 rescued the respiratory chain defect in patient-derived myoblasts. First, we measured enzyme activities of each mitochondrial respiratory complex in mitochondrial fractions prepared from immortalized patient-derived myoblasts. CS activity normalized values for complexes I, IV, and V activity in immortalized patient-derived myoblasts were decreased to 17%, 39%, and 43% of the mean values of immortalized control myoblasts (Fig. 5C). Then, we measured enzyme activity in mitochondrial fractions prepared from rescued myoblasts and found that each activity of complexes I, IV, and V was mostly restored relative to that in vector-only myoblasts. In rescued myoblasts, CS activity normalized values of complexes I, IV, and V were 3.5, 1.3, and 2.2 times higher than those in vector-only myoblasts (Fig. 5C). Mitochondrial respiratory complex activity was mostly restored in rescued myoblasts, suggesting that there was an unidentified link between deficiency of ECHS1 and respiratory chain.